








# Zfp580 inactivation as a new therapeutic target to enhance recovery after stroke in mice

Christian J Hoffmann<sup>1,2</sup> , Melanie TC Kuffner<sup>1,2</sup>,  
Leif Koschützke<sup>1,2</sup> , Stephanie Lorenz<sup>1</sup>, Janet Lips<sup>1,2</sup>,  
Philipp Boehm-Sturm<sup>1,2,3</sup> , Susanne Mueller<sup>1,2,3</sup>,  
Stefan P Koch<sup>1,2,3</sup>, Jeehye An<sup>1,2,3</sup> , Lucius S Fekonja<sup>1,2,3</sup>,  
Polina Bugaeva<sup>1,2,4</sup>, Andre Rex<sup>1</sup>, Gisela Lättig Tünnemann<sup>1,2</sup>,  
Matthias Endres<sup>1,2,4,5,6,7</sup> and Christoph Harms<sup>1,2,4,5</sup> 

## Abstract

Paracrine cerebral Interleukin 6 (Il6) is relevant for stroke recovery, but systemic Il6 elevation may worsen outcome. Hence, paracrine Il6 response modulation within the neurovascular unit has emerged as an attractive therapeutic approach. Lithium modulates Il6 responses and improves stroke outcome. However, lithium may cause serious adverse effects. Here, we report that Zincfinger protein 580 (Zfp580) mediates the effects of lithium on Il6 signaling. In contrast to lithium, Zfp580 inactivation had no neurotoxic effects, and Zfp580 knock out mice showed no phenotypic changes in cognitive and motor function behavioral tests. We discovered that lithium and hypoxia disinhibited Il6 via Zfp580 suppression and post-translational modification by small ubiquitin-like modifier (SUMO). After transient middle cerebral artery occlusion, loss of Zfp580 reduced paracrine Il6 and increased Il6 trans-signaling. Aside from modulating Il6 signaling, Zfp580 loss improved endothelial resilience to ischemia, was highly neuroprotective resulting in smaller infarcts and enhanced use-dependent neuroplasticity, all of which led to improved functional outcome. In conclusion, inactivation of Zfp580 exerts positive effects on multiple key mechanisms without exhibiting relevant adverse side effects, making it potentially a more specific and effective treatment target for stroke recovery than lithium. To fully assess its potential, Zfp580 inhibitors must be developed.

## Keywords

Il6 signaling, Zfp580, stroke, use-dependent plasticity, stroke recovery

Received 15 February 2022; Revised 3 March 2023; Accepted 10 March 2023

## Introduction

Stroke long-term outcome is influenced by several factors, including brain protection in acute ischemia and postischemic repair mechanisms such as compensation,

plasticity, and tissue remodeling to regain lost functions. Local paracrine interactions of neurons, glia, and vascular cells within the neurovascular unit have

<sup>1</sup>Klinik und Hochschulambulanz für Neurologie mit Experimenteller Neurologie, Charité-Universitätsmedizin Berlin, Corporate Member of Freie Universität Berlin, Humboldt-Universität zu Berlin, and Berlin Institute of Health

<sup>2</sup>Center for Stroke Research Berlin, Charité-Universitätsmedizin Berlin, Berlin, Germany

<sup>3</sup>NeuroCure Cluster of Excellence and Charité Core Facility 7T Experimental MRIs, Charité-Universitätsmedizin Berlin, Berlin, Germany

<sup>4</sup>Einstein Center for Neuroscience, Berlin, Germany

<sup>5</sup>German Center for Cardiovascular Research (DZHK), partner site Berlin, Germany

<sup>6</sup>NeuroCure Clinical Research Center, Charité-Universitätsmedizin Berlin, Berlin, Germany

<sup>7</sup>German Center for Neurodegenerative Diseases (DZNE), partner site Berlin, Germany

## Corresponding authors:

Christian J Hoffmann, Charité-Universitätsmedizin Berlin, Robert-Koch-Platz 4, 10115 Berlin, Germany.  
Email: christian.hoffmann@charite.de

Christoph Harms, Charité-Universitätsmedizin Berlin, Robert-Koch-Platz 4, 10115 Berlin, Germany.  
Email: christoph.harms@charite.de

a significant impact on these mechanisms, and the cytokine Interleukin 6 (Il6) is important in such processes.<sup>1,2</sup>

Since the Il6 receptor (Il6r) lacks a catalytic domain, a complex of Il6 and Il6r with glycoprotein 130 (gp130) is required for classical signaling.<sup>3</sup> Furthermore, Il6 can activate down-stream signaling via trans-signaling in cells lacking Il6r: a soluble form of the Il6 receptor (sIl6r) can bind Il6 and gp130, which is ubiquitously expressed. Additionally, soluble gp130 (sgp130) can inhibit trans-signaling but not classical signaling. The effects of classical signaling differ from those of trans-signaling: Classical signaling induces anti-inflammatory effects, whereas trans-signaling induces its pro-inflammatory effects.<sup>4</sup> However, after cerebral damage, Il6 trans-signaling can induce repair mechanisms and improve functional outcome.<sup>5,6</sup> We have shown that Il6-induced postischemic angiogenesis is a major contributor to stroke repair processes,<sup>1</sup> and that downstream signaling in endothelial cells by Signal transducer and activator of transcription 3 (Stat3) induces changes in the neurovascular unit's microenvironment, improving neuroplasticity and functional outcome.<sup>7</sup> However, increased Il6 blood levels are strongly associated with a worse outcome in stroke patients, though it is unclear whether this is a causal contribution.<sup>8</sup> Increasing systemic Il6 does not appear to be a viable treatment option, however, because signaling is complex, and effects vary greatly depending on temporal and spatial expression, as well as the balance of classical and trans-signaling. Instead, it may be advantageous to specifically modulate paracrine Il6 classical and trans-signaling within ischemic brain tissue.

Lithium is a drug known to modulate Il6 signaling: In patients with bipolar disorder, lithium normalizes elevated Il6 production of monocytes, and in healthy controls, it increases sIl6r blood levels.<sup>9,10</sup> Lithium treatment has favorable effects on motor function recovery and angiogenesis after stroke,<sup>11,12</sup> though effects on endothelial cells have rarely been studied and are controversial.<sup>13–16</sup> However, lithium's narrow therapeutic window and potential serious side effects are disadvantages. Zincfinger protein 580 (Zfp580) suppresses Interleukin 8 in endothelial cells and Il6 in monocytes<sup>17,18</sup> and enhances proliferation and migration of endothelial cells by inducing Vegf and Mmp2 expression.<sup>19–21</sup> Zfp580 is protective against hypoxia *in vitro* in a rat cardiomyoblastic<sup>22</sup> and a human neuroblastoma cell line.<sup>23</sup>

This study aimed to investigate whether Zfp580 is a downstream target of lithium mediating its effects on Il6 signaling, whether Zfp580 modulates paracrine Il6 signaling after stroke and how it affects stroke outcome.

## Materials and methods

### Study design

This study aimed to identify a new downstream target of lithium that modulates paracrine cerebral Il6 signaling to enhance stroke recovery. Therefore, we examined the effects of lithium on Zfp580 and Il6 *in vitro* before focusing on Zfp580 in *in vivo* studies. We used Zfp580 knockout mice in the stroke model of transient middle cerebral artery occlusion to evaluate the effects on paracrine cerebral and systemic Il6, Il6 trans-signaling, angiogenesis, ischemic lesion size and functional recovery. Sample sizes were determined by power-analyses (for details see Supplemental material) using G\*Power software and were indicated by dots in the figures.

### Cell culture

Brain microvascular endothelial cells (bEnd.3, ATCC CRL-2299, Manassas, VA, USA) were purchased from ATCC. Experiments were done at 100% confluency. The different modified cell clones were generated using lentiviral particles.<sup>24</sup> Primary neurons were derived from C57BL/6 mice at E15.<sup>24</sup>

### Real-time RT-PCR

Real-time RT-PCR was performed as described.<sup>7</sup> Primers are listed in Supplemental Table 1 in the online-only Data Supplement.

### Immunoblotting

Immunoblotting was performed using primary antibodies for Zfp580 produced in goat (1:1000, Santa Cruz, USA) directed against the C-terminus or produced in rabbit (1:500, Antikoerper-online.de, ABIN1538689, Aachen, Germany) directed against the middle region or for SUMO2/3 produced in rabbit (1:1000, Invitrogen, #519100, Carlsbad, CA, USA).

### Enzyme-linked immunosorbent assay

ELISAs to determine Il6 (Invitrogen, KMC0061, Waltham, MA, USA) levels in cell culture supernatants, Il6 (R&D Systems, M6000B, Minneapolis, MN, USA) or sIl6r (R&D Systems, DY1830) were performed according to the manufacturer's instructions. The binary Il6:Il6r complex was quantified as previously described.<sup>25</sup>

### Tandem affinity purification

A bEnd.3 cell clone expressing a construct for the simultaneous tandem affinity purification of SUMO1,

SUMO2 and SUMO3 was generated by lentiviral transduction. After purification, immunoblotting for Zfp580 was performed as described above using the Zfp580 antibody produced in goat.

### *Fractionation of cytosolic and nuclear proteins*

Cellular fractionation was performed as described in the online-only Data Supplement.

### *Immunofluorescence staining*

Cells were stained with anti-Zfp580 antibody (Sigma Aldrich, Prestige antibodies™, rabbit, HPA054058, St. Louis, MO, USA) and brain slices with anti-Zfp580 antibody (Antikoerper-online.de, ABIN153 8689, Aachen, Germany). Confocal images were collected with a Leica SP8 microscope.

### *Scratch wound migration and proliferation assay*

Cells were grown to confluence in 48-well plates. A scratch wound was applied to the monolayer using a 20- $\mu$ l pipette tip. Images were taken immediately after wounding and after 24 h or 48 h at the same location. Shown are percentages of the gap width remaining.

For proliferation assay, cells were incubated for with BrdU and stained for incorporated BrdU after 48 h.

### *Oxygen and glucose deprivation (OGD)*

Endothelial cells and primary neurons were subjected to combined OGD as described previously.<sup>26</sup>

### *Cell survival and lactate dehydrogenase assay*

Surviving neurons were counted using epifluorescence images before (DIV8) and 24 h after OGD as described<sup>24</sup> and surviving endothelial cells 24 h after OGD.

Lactate dehydrogenase (LDH) was performed following a published protocol.<sup>27</sup>

### *Animals*

All experimental procedures were conducted following the German Animal Welfare Act and Animal Welfare Regulation Governing Experimental Animals – TierSchVersV) and approved by the State Office for Health and Social Affairs (LaGeSo) under licence number G0254/16. Zfp580tm1a<sup>(EUCOMM)Wtsi</sup> mice (constitutive Zfp580 knockout mice, C57/BL6/N background) were purchased from EuMMCR (Helmholtz Zentrum München).

### *Mouse modeling and transient middle cerebral artery occlusion (MCAo)*

Mice underwent transient filamentous occlusion of the middle cerebral artery for 45 min according to a published standard operating procedure from our laboratory.<sup>28</sup>

### *Magnetic resonance imaging*

T2-weighted images were acquired 24-h after MCAo. MRI data were registered on the mouse Allen Brain Atlas (ABA) using in-house developed MATLAB toolbox ANTx2 (<https://github.com/ChariteExpMri/antx2>). Incidence maps expressing the percentage of animals with a lesion in a voxel were plotted for each group in atlas space, and edema-corrected lesion volumes were calculated as described previously.<sup>29</sup> After 21 days, T2-weighted and diffusion MRI (dMRI) were performed as outlined in detail in the Expanded Methods section.

### *Behavioral tests*

Rotarod or modified DeSimoni Neuroscore were performed as previously described.<sup>30</sup>

To assess the fine motor function of the forepaws, we used the staircase test as previously described.<sup>31</sup> Results obtained on 14 consecutive days before stroke were averaged as the baseline for each animal and side. After stroke, the side-specific performances of the forepaws were normalized to this skill level.

Novel object recognition and Y-Maze were performed as described previously.<sup>32,33</sup>

### *Histology and determination of lesion size*

Staining for caveolin-1 or NeuN were done using the Avidin/Biotin blocking kit and DAB substrate kit (Vector Laboratories, Newark, CA, USA) according to the manufacturer's protocol. Vessel density and NeuN lesion size were evaluated using ImageJ software (National Institutes of Health, Bethesda, MD). NeuN lesion size was calculated by summing the infarct sizes as previously described using the indirect lesion size.<sup>28</sup>

### *Methods to prevent bias*

The experimenters were blinded to all experiments, which required manual rating. Group allocation was concealed for behavioral tests. Animals were randomized for MCAo operation, and experimenters were blinded to the genotype. Reporting conforms to the ARRIVE guidelines.

## Statistical analyses

All data were tested for normal distribution using the Shapiro-Wilk test. Variance homogeneity was assessed using F-test or Brown-Forsythe test. The data are presented as scatter dot plots, normal distributed data with the mean  $\pm$  standard deviation and not normal distributed data with median  $\pm$  interquartile range. Data were analyzed with GraphPad Prism version 8.2.0. A detailed description of the corresponding statistical analysis is provided in the figure legends.

## Results

### *Zfp580 is expressed in endothelial cells and neurons and inhibits Il6*

First, we evaluated whether Zfp580 is expressed in endothelial cells and neurons as primary cells of the neurovascular unit. Zfp580 mRNA was expressed in both neuronal and endothelial cells, with higher expression levels in neurons (Figure 1(a)). Immunofluorescence staining revealed that Zfp580 was predominantly nuclear in both cell types (Figure 2(b)). It is known that Zfp580 inhibits Il6 in monocytes. To determine whether it also suppresses Il6 in endothelial cells, we generated bEnd.3 cell clones with either increased expression of wild-type Zfp580 (wtZfp580) or Zfp580 knock down by lentiviral transduction using two different miRNA-embedded small hairpin RNAs (shRNAs). An shRNA directed against the prokaryotic LacZ gene product  $\beta$ -galactosidase served as a negative control for knock-down. We achieved a strong increase in Zfp580 by exogenous expression (Supplemental Figure 1(a)). Increased Zfp580 expression inhibited Il6 mRNA expression and Il6 protein secretion in bEnd.3 cells compared to unmodified cells (Figure 1(c) and (d)). Both shRNAs knocked down Zfp580 efficiently (Supplemental Figure 1(b)). Il6 was induced at the mRNA and protein levels upon Zfp580 knockdown (Figure 1(e) and (f)). Hence, Zfp580 suppressed Il6 in endothelial cells.

### *Zfp580 mediates the effect of lithium on Il6*

We then evaluated whether Zfp580 mediates the effect of lithium on Il6. The cells were exposed to lithium chloride (LiCl) or sodium chloride (NaCl) as negative control. Zfp580 expression was time- and dose-dependently suppressed by LiCl, with early suppression beginning at 3 h after exposure, and this suppression was sustained for at least 24 h (Figure 1(g) and (h)). In contrast, Il6 was time- and dose-dependently induced by LiCl (Figure 1(i) and (j)). Il6 induction occurred fast, beginning at 3 h after exposure. Given that LiCl is a Gsk3 inhibitor, we investigated whether

Gsk3 is necessary for LiCl's impact on Zfp580 and Il6 expression. In order to effectively inactivate Gsk3 prior to LiCl treatment, we exposed the cells to the specific Gsk3 inhibitor CHIR99021. CHIR99021 by itself had no effect on Zfp580 expression, and CHIR99021 treatment prior to LiCl treatment had no effect on LiCl-induced Zfp580 suppression. (Figure 1(k)). Therefore, the Zfp580 suppressive effect of LiCl did not depend on Gsk3. Gsk3 inactivation, however, prevented LiCl from having any additional Il6 inducing effects (Figure 1(l)). Instead, additional LiCl treatment lessened CHIR99021's ability to induce Il6. We knocked down Zfp580 prior to LiCl or CHIR99021 treatment in order to ascertain whether Zfp580 mediates the effects of these agents on Il6. This prevented LiCl or CHIR99021 from inducing Il6 (Figure 1(m) and (n)). In neurons, we observed similar effects: LiCl suppressed Zfp580 (Figure 1(o)) and induced Il6 strongly (Figure 1(p)). CHIR99021 treatment had no effect on Zfp580 expression (Figure 1(q)) but strongly induced Il6 (Figure 1(r)). In summary, LiCl suppresses Zfp580 Gsk3 independently in cerebral microvascular endothelial cells and neurons as principal cells of the neurovascular unit. Additionally, Zfp580 mediates the Gsk3 dependent effects of LiCl on Il6 expression.

### *Lithium inactivates Zfp580 by inducing its degradation, SUMOylation and nuclear exclusion*

We identified additional Zfp580 bands in the immunoblot with molecular weights ranging from approximately 18 to 130 kD that were reduced in shRNA-expressing cells (Figure 2(a) and Supplemental Figure 3(a)). Zfp580's amino acid sequence is highly conserved across species, with only five amino acids separating Zfp580 from humans, mice, and rats. (Supplemental Figure 2(a)). A yet uncharacterized SUMO consensus site with the sequence PKAE (amino acids 30–33) is present in the N-terminal domain of Zfp580 (Supplemental Figure 2(a), marked in gray). SUMO is a post-translational modifier that is covalently bound to a lysine (K) within the SUMO consensus site. Three functional isoforms of SUMO (SUMO1–3) have been described in the brain and in endothelial cells so far, and these isoforms can build poly-SUMO chains.<sup>34</sup> To determine whether SUMOylation modifies Zfp580 post-translationally, we created a bEnd.3 cell clone expressing a construct for all three SUMO variants (SUMO1–3) for tandem affinity purification. After purification, we immunoblotted the highly purified SUMO proteins with their covalently bound conjugates and stained for Zfp580. We identified the bands with 24 kD, 35 kD, 50 kD, 70 kD, 100 kD and 130 kD as SUMOylated Zfp580 variants (Figure 2(b) and Supplemental Figure 3(b)). We next determined the



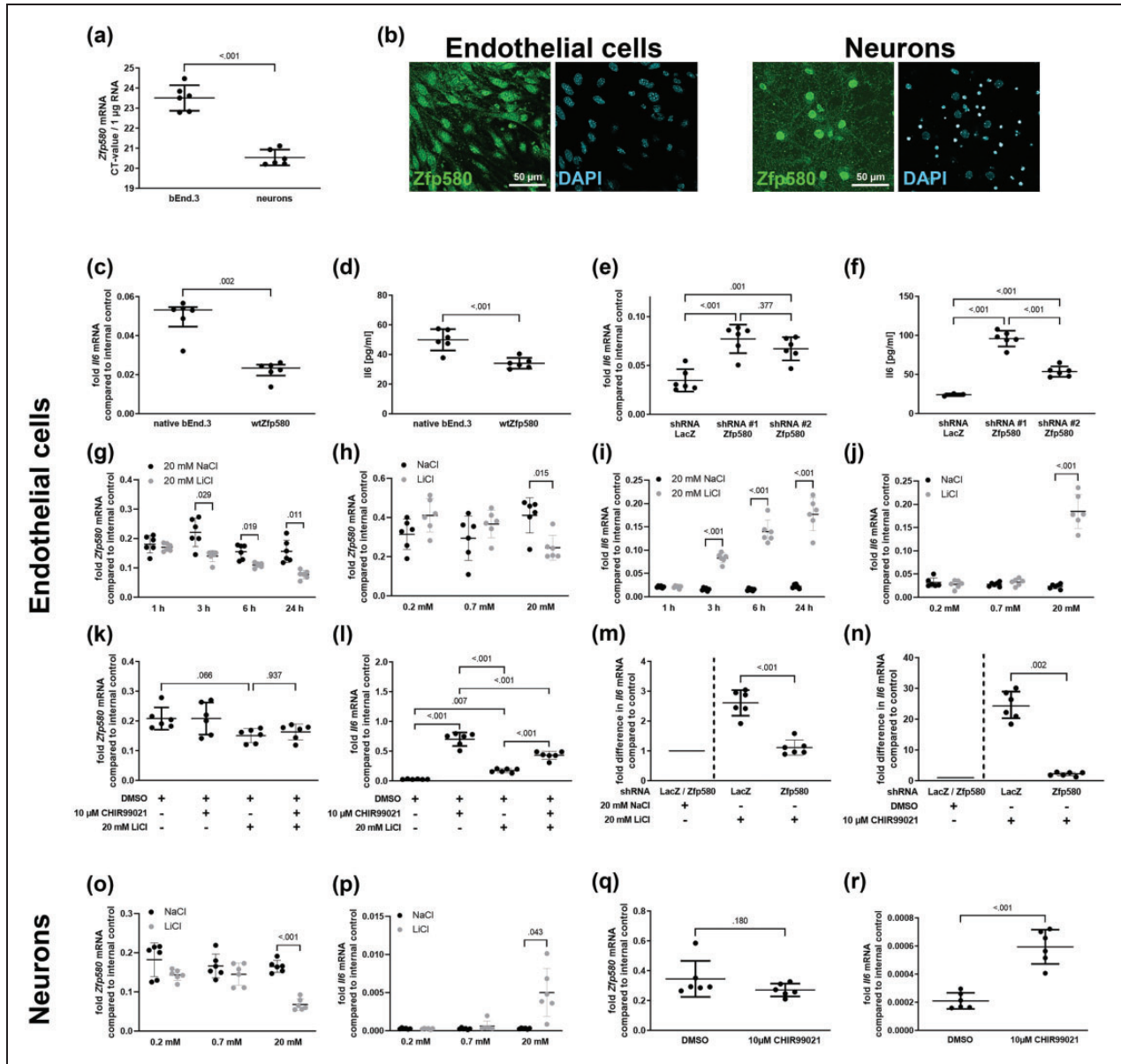


**Figure 1.** The induction of Il6 by lithium or Gsk3 inhibition is mediated by Zfp580, which is an inhibitor of Il6. (a) Expression levels of Il6 in microvascular cerebral endothelial cells (bEnd.3) or neurons determined by real-time RT-PCR. Presented is the Il6 CT-value derived from 1  $\mu$ g total RNA. Neurons express Zfp580 at a higher level than endothelial cells. (two-tailed unpaired Student's *t*-test:  $t(10) = 9.733$ ,  $p < .001$ ). (b) Immunofluorescence staining of Zfp580 in bEnd.3 and neurons. Zfp580 is mostly found in the nucleus. Endothelial cells with increased expression ((c) and (d)) or knockdown of Zfp580 due to the use of two different miRNA-embedded shRNAs ((e) and (f)) were generated by lentiviral transduction. The mRNA expression of Il6 was determined by real-time RT-PCR. Il6 protein levels in the cell culture supernatant were determined by ELISA. Increased expression of Zfp580 led to suppression of Il6 mRNA (c) (Mann-Whitney test:  $p = .002$ ) and secretion of the Il6 protein (d) (two-tailed unpaired Student's *t*-test:  $t(10) = 4.816$ ,  $p < .001$ ). Knockdown of Zfp580 induced Il6 mRNA (e) (One-way ANOVA with Sidak's multiple comparison test:  $F(2,15) = 140.9$ ,  $p < .001$ ) and Il6 secretion (f) (One-way ANOVA with Tukey's multiple comparison test:  $F(2,12) = 94.02$ ,  $p < .001$ ). We analyzed the time and dose dependent effect of lithium chloride (LiCl) on Zfp580 and Il6 expression levels compared to cells exposed to sodium chloride (NaCl) using a two-way RM ANOVA with Sidak's multiple comparison test and Geisser-Greenhouse correction. In endothelial cells, LiCl suppressed Zfp580 mRNA expression in a time-dependent manner (g) depending on time point, LiCl treatment and the interaction between both factors ( $F(2.636, 26.36) = 24.63$ ,  $p < .001$ ;  $F(1, 10) = 21.88$ ,  $p < 0.001$ ;  $F(3, 30) = 6.924$ ,  $p = .001$ ), and dose-dependent manner (h) depending on the interaction between dosage and LiCl treatment ( $F(2, 20) = 7.881$ ,  $p = .003$ ). LiCl increased Il6 mRNA expression in a time-dependent manner (i) depending on time point, LiCl treatment and the interaction between both factors ( $F(1.118, 11.18) = 43.16$ ,  $p < .001$ ;  $F(1, 10) = 2098$ ,  $p < 0.001$ ;  $F(3, 30) = 43.54$ ,  $p < .001$ ), and dose-dependent manner (j) depending on dosage, LiCl treatment and interaction between both factors ( $F(1.218, 12.18) = 77.65$ ,  $p < .001$ ;  $F(1, 10) = 109.1$ ,

Continued.

effect of LiCl on Zfp580 protein levels and SUMOylation. The cells were exposed to either 0.2 mM, 0.7 mM and 20 mM NaCl or LiCl for 24 h and immunoblotted for Zfp580. Both NaCl and LiCl reduced Zfp580 protein levels, including all SUMOylated variants, but LiCl to a greater extent than NaCl (Figure 2(c) and Supplemental Figure 3(c)). Treatment with CHIR99021 showed a similar effect (Figure 2(d) and Supplemental Figure 3(d)). To ascertain whether the effect of LiCl on Il6 expression depends solely on Zfp580 protein level reduction or also on Zfp580 SUMOylation, we pretreated the cells with the specific SUMOylation inhibitor TAK-981 4 hours before LiCl treatment. TAK-981 diminished the inductive effect of LiCl on Il6 but did not eliminate it (Figure 2(e)). Therefore, the effect of LiCl on Il6 depends on both, Zfp580 degradation and SUMOylation. To assess the effect of Zfp580 SUMOylation, we separated the nuclear and cytosolic proteins and discovered that the 130-kD and 55-kD variants of Zfp580 were cytosolic, while the 35-kD, 24-kD, and unmodified 18-kD variants were nuclear (Figure 2(f) and Supplemental Figure 3(e)). We generated a bEnd.3 cell clone expressing a mutant form of Zfp580 in which the lysine residue within the predicted SUMOylation site was mutated to an arginine (Zfp580K31R). In this cell clone, endogenous wild-type Zfp580 was retained, but overexpression of the Zfp580K31R mutant greatly reduced bands at molecular weights of 24-kD to 130-kD (Figure 2(f) and Supplemental Figure 3(e)). This indicates that Zfp580 is SUMOylated at the lysine residue at position 31 within the predicted SUMO consensus site and that poly-SUMOylated Zfp580 is located in the cytosol. Translocation of the SUMOylated transcription factor Zfp580 to the cytosol would cause its inactivation. In immunofluorescence stainings for Zfp580 after exposure to increasing concentrations of LiCl, we observed a dose-dependent nuclear exclusion of Zfp580 (Figure 2(g)).

Increased wtZfp580 expression resulted in increased nuclear Zfp580 (Figure 2(h)). Unexpectedly, Zfp580 condensed at particular locations inside the nucleus. While NaCl had no effect, LiCl effectively excluded Zfp580 from the nucleus while the condensed nuclear spots persisted. Comparing the effect of 20 mM NaCl or LiCl on native bEnd.3, increased wtZfp580 expressing, and Zfp580K31R expressing cells, most prominently the mono-SUMOylated nuclear 24-kD variant is increased by LiCl and wtZfp580 overexpression, whereas it is absent in Zfp580K31R cells (Figure 2(i) and Supplemental Figure 3(g)). Additionally, LiCl increased the cytosolic >70-kD variants in native bEnd.3 and wtZfp580 expressing cells. In Zfp580K31R cells, Zfp580 is drastically reduced, and there is no discernible difference between cells treated with NaCl or LiCl. When wtZfp580 cells are compared to native bEnd.3, Il6 disinhibition on mRNA (Figure 2(j)) and secreted protein level (Figure 2(k)) is increased, and this is most pronounced in Zfp580K31R cells. A similar effect was observed with CHIR99021 treatment (Figure 2(l) and (m)). Notably, lithium had no effect on global protein SUMOylation: there was no difference in SUMO2/3 in the immunoblot after treatment with 20 mM NaCl or LiCl (Figure 2(n) and Supplemental Figure 3(h)). Rather, lithium specifically induced Zfp580 SUMOylation. Taken together, these results show that LiCl induced Zfp580 degradation and SUMOylation at the lysine at position 31, resulting in nuclear exclusion and condensation at distinct presumably inactive spots in the nucleus and, therefore, Zfp580 inactivation. These mechanisms are involved in the upregulation of Il6 by lithium.

### *Zfp580 increases and lithium inhibits endothelial cell migration mediated by Il6 trans-signaling*

To evaluate the effect of lithium and Zfp580 on endothelial cell migration, we used the scratch wound assay.

#### **Figure 1.** Continued.

$p < 0.001$ ;  $F(2,20) = 91.59$ ,  $p < .001$ ). To determine whether the effect of LiCl on Zfp580 and Il6 expression is dependent on Gsk3, we inactivated Gsk3 prior to LiCl treatment by incubating the cells with the specific Gsk3 inhibitor CHIR99021. CHIR99021 had no effect on Zfp580 expression (k), but induced Il6 more than lithium treatment ( $p < .001$ ) (l). LiCl showed no additional Il6 inductive effect after CHIR99021 treatment. Instead, CHIR99021's Il6 inductive effect was significantly diminished when combined with lithium. ( $p < .001$ ) (One-way ANOVA with Tukey's multiple comparison test:  $F(3, 20) = 115.7$ ,  $p < .001$ ). To determine whether Zfp580 mediates the effects of LiCl and CHIR99021 on Il6 expression, we knocked down Zfp580 prior to lithium (m) or CHIR99021 (n) treatment. Presented is the fold increase in Il6 mRNA compared to the respective NaCl or DMSO control. Compared to cells expressing LacZ-shRNA, knock down of Zfp580 strongly reduced the inductive effect of LiCl (two-tailed unpaired Student's t-test:  $t(10) = 7.380$ ,  $p < .001$ ) and CHIR99021 (Mann-Whitney test:  $p = .002$ ). In neurons as second principal cells of the neurovascular unit, we observed similar effects: LiCl suppressed Zfp580 mRNA expression in a dose-dependent manner (o) depending on dosage, LiCl treatment and the interaction between both factors ( $F(1.810, 18.10) = 6.287$ ,  $p = .002$ ;  $F(1, 10) = 41.97$ ,  $p < 0.001$ ;  $F(2, 20) = 6.287$ ,  $p = .008$ ). LiCl increased Il6 mRNA expression in a dose-dependent manner (p) depending on dosage, LiCl treatment and interaction between both factors ( $F(1.051, 10.51) = 11.90$ ,  $p = .005$ ;  $F(1, 10) = 15.23$ ,  $p = 0.003$ ;  $F(2,20) = 11.70$ ,  $p < .001$ ). Incubating neurons with 10  $\mu$ M CHIR99021 for 24 h had no effect on Zfp580 expression (q), but strongly induced Il6 and (r) (two-tailed unpaired Student's t-test:  $t(10) = 7.004$ ,  $p < .001$ ). Graphs show scatter dot plots of independent experiments and means  $\pm$  standard deviation except (c) showing median  $\pm$  interquartile range.

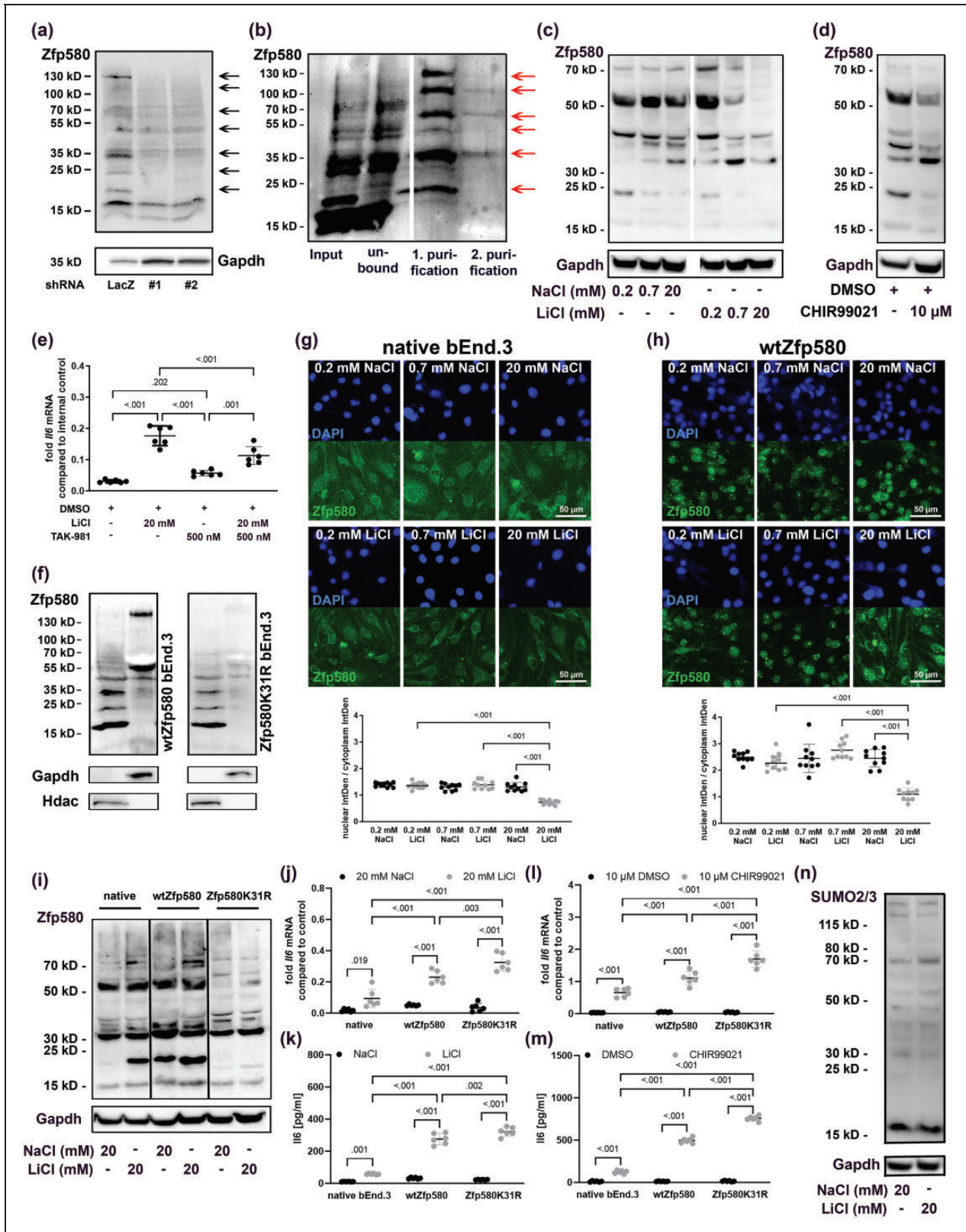


**Figure 2.** Lithium inactivates Zfp580 by inducing its degradation, SUMOylation and nuclear exclusion. (a) In bEnd.3 cells, we identified additional Zfp580 bands in the immunoblot with molecular weights between approximately 18 and 130 kD which were reduced by Zfp580-RNAi. (b) Tandem affinity purification using FPLC of equimolar SUMO1-3 from a single vector. Each SUMO variant was fused to a His-tag and an S-tag. First, purification was based on the His-tag, after which a second purification step for the S-tag was performed. (c) Zfp580 immunoblot in bEnd.3 cells treated with NaCl (0.2, 0.7, 20 mM) and LiCl (0.2, 0.7, 20 mM). (d) Zfp580 immunoblot in bEnd.3 cells treated with DMSO or CHIR99021 (10 μM). (e) Dot plot of fold IIF mRNA compared to internal control. (f) Western blot for Zfp580, Gapdh, and Hdac in wtZfp580 and Zfp580K31R bEnd.3 cells. (g) Immunofluorescence for native bEnd.3 cells treated with NaCl (0.2, 0.7, 20 mM) or LiCl (0.2, 0.7, 20 mM). (h) Immunofluorescence for wtZfp580 cells treated with NaCl (0.2, 0.7, 20 mM) or LiCl (0.2, 0.7, 20 mM). (i) Immunoblot for Zfp580 in native, wtZfp580, and Zfp580K31R cells treated with NaCl (20 mM) and LiCl (20 mM). (j) Dot plot of fold IIF mRNA compared to control for native, wtZfp580, and Zfp580K31R cells. (k) Dot plot of IIF [pg/ml] for native bEnd.3, wtZfp580, and Zfp580K31R cells. (l) Dot plot of fold IIF mRNA compared to control for native, wtZfp580, and Zfp580K31R cells treated with DMSO or CHIR99021 (10 μM). (m) Immunoblot for SUMO2/3 in native bEnd.3, wtZfp580, and Zfp580K31R cells treated with DMSO or CHIR99021 (10 μM). (n) Dot plot of fold IIF mRNA compared to control for SUMO2/3 cells treated with NaCl (20 mM) and LiCl (20 mM). Continued.



Increased Zfp580 expression accelerated endothelial cell migration compared to untreated bEnd.3 cells (Figure 3(a) and Supplemental Figure 4(a)). Consistently, Zfp580 knock down reduced endothelial cell migration (Figure 3(b) and Supplemental Figure 4 (b)). Furthermore, lithium reduced endothelial cell migration (Figure 3(c) and Supplemental Figure 4(c)). These findings were surprising since both Zfp580 knockdown and lithium treatment induced Il6, which is known to increase endothelial cell migration via classical Il6 signaling. In order to determine whether Il6 trans-signaling mediates the inhibition of endothelial cell migration, we selectively inhibited Il6 trans-signaling by adding sgp130 to the culture medium. Inhibition of Il6 trans-signaling with sgp130 dose-dependently reduced the migration inhibitory effect of Zfp580 knockdown (Figure 3(d) and Supplemental Figure 4(d)) or LiCl treatment (Figure 3(e) and Supplemental Figure 4(e)). This was not the case in the control groups of cells expressing LacZ shRNA cells or treated with NaCl. Therefore, lithium and Zfp580 knockdown inhibited endothelial cell migration, which was mediated by Il6 induction and Il6 trans-signaling.

### Lithium blocks endothelial cell migration by the SUMOylation of Zfp580

To assess, whether Zfp580 mediates the effects of LiCl on migration, we exposed cells with Zfp580 knock down to 20 mM LiCl. After knock down of Zfp580, LiCl had no effect on migration (Figure 3(f) and Supplemental Figure 4(f)). Increased expression of wtZfp580 induced endothelial cell migration (Figure 3(g) and Supplemental Figure 4(g)). Zfp580K31R increased migration to a greater extent than wtZfp580. Increased expression of wtZfp580 did not block the inhibitory effect of lithium on endothelial cell migration. The Zfp580K31R mutant completely blocked the effect of LiCl on migration (Figure 3(g)) and Il6 trans-signaling inhibition by sgp130 showed no further effect on endothelial cell migration in Zfp580K31R cells (Figure 3(h)). Thus, Zfp580 mediates the effect of lithium on migration as depicted in Figure 3(i). Lithium suppresses Zfp580 and inactivates Zfp580 by the SUMOylation of Zfp580 at K31. This leads to Il6 induction and the inhibition of endothelial cell migration by Il6 trans-signaling.

#### Figure 2. Continued.

carried out, and subsequent immunoblotting for Zfp580 was performed. Six bands corresponding to molecular weights of 24 kD, 35 kD, 50 kD, 70 kD, 100 kD and 130 kD were detectable, indicating the covalent SUMOylation of Zfp580. (c) Zfp580 immunoblot of cells treated with 0.2 mM, 0.7 mM or 20 mM NaCl or LiCl for 24 h. Both, NaCl and LiCl suppressed Zfp580 protein level, but LiCl to a higher extent. (d) Zfp580 immunoblot of cells treated with 10  $\mu$ M CHIR99021 or DMSO for 24 h. CHIR99021 suppressed Zfp580 protein levels. (e) To determine whether the effect of LiCl on Il6 depends on the SUMOylation of Zfp580, SUMOylation was inhibited 4 h prior to LiCl treatment using 500 mM TAK-981, and Il6 expression was measured using real-time RT-PCR. TAK-981 diminished the inductive effect of LiCl on Il6 but did not eliminate it ( $p < .001$ ) (Brown-Fortsythe ANOVA with Tukey's multiple comparison test:  $F^*(3, 11.32) = 286.3, p < .001$ ). (f) Fractionation of cytosolic and nuclear proteins from wild-type bEnd.3 cells and Zfp580K31R-expressing bEnd.3 cells. The 130-kD and 55-kD variants of Zfp580 are detectable in the cytosol, and the 35-kD, 24-kD and unmodified 18-kD variants were detectable in the nucleus. Mutation of the predicted SUMOylation motif at K31 led to reductions in the higher molecular-weight variants. (g) Immunofluorescence staining for Zfp580 in bEnd.3 cells treated with 0.2 mM, 0.7 mM or 20 mM NaCl or LiCl for 24 h. NaCl treatment showed no effect whereas Zfp580 was dose-dependently excluded from the nucleus after LiCl treatment (One-way ANOVA with Tukey's multiple comparison test:  $F(5, 54) = 40.54, p < .001$ ). (h) Immunofluorescence staining for Zfp580 in increased wtZfp580 expressing cells treated with 0.2 mM, 0.7 mM or 20 mM NaCl or LiCl for 24 h. Exogenous wtZfp580 expression resulted in increased nuclear Zfp580; however, NaCl treatment had no effect, whereas LiCl treatment dose-dependently excluded Zfp580 from the nucleus (One-way ANOVA with Tukey's multiple comparison test:  $F(5, 54) = 30.14, p < .001$ ). (i) Zfp580 immunoblot of native bEnd.3, wtZfp580 expressing cells or Zfp580K31R expressing cells treated either with 20 mM NaCl or 20 mM LiCl for 24 h. LiCl induced the nuclear mono-SUMOylated 24-kD band and the cytosolic >70-kD variants in native bEnd.3 and wtZfp580 expressing cells. Zfp580 is drastically reduced in Zfp580K31R cells, and there is no discernible difference between cells treated with NaCl or LiCl. Notably, the 24-kD nuclear mono-SUMOylated band is totally absent. (j) - (m) Comparison of Il6 expression (real-time RT-PCR) and secretion (ELISA) in native bEnd.3, wtZfp580 expressing, and Zfp580K31R expressing cells following LiCl or CHIR99021 treatment using a two-way ANOVA with Tukey's multiple comparison test. Il6 disinhibition is increased in wtZfp580 cells and is most pronounced in Zfp580K31R cells. (j) LiCl disinhibited Il6 mRNA expression depending on the Zfp580 variant, LiCl treatment and the interaction between both factors ( $F(2, 30) = 32.8, p < .001$ ;  $F(1, 30) = 199.9, p < 0.001$ ;  $F(2, 30) = 22.72, p < .001$ ) and (k) secreted Il6 protein depending on the Zfp580 variant, LiCl treatment and the interaction between both factors ( $F(2, 30) = 203.2, p < .001$ ;  $F(1, 30) = 1055, p < 0.001$ ;  $F(2, 30) = 158.6, p < .001$ ). (l) CHIR99021 disinhibited Il6 mRNA expression depending on the Zfp580 variant, CHIR99021 treatment and the interaction between both factors ( $F(2, 30) = 39.92, p < .001$ ;  $F(1, 30) = 529.4, p < 0.001$ ;  $F(2, 30) = 38.46, p < .001$ ) and (m) secreted Il6 protein depending on the Zfp580 variant, CHIR99021 treatment and the interaction between both factors ( $F(2, 30) = 819.1, p < .001$ ;  $F(1, 30) = 4762, p < 0.001$ ;  $F(2, 30) = 802.1, p < .001$ ) and (n) SUMO2/3 immunoblot of bEnd.3 exposed to 20 mM NaCl or LiCl for 24 h. LiCl did not induce global SUMOylation of proteins. The Graph shows a scatter dot plot of the mean of independent experiments  $\pm$  standard deviations.



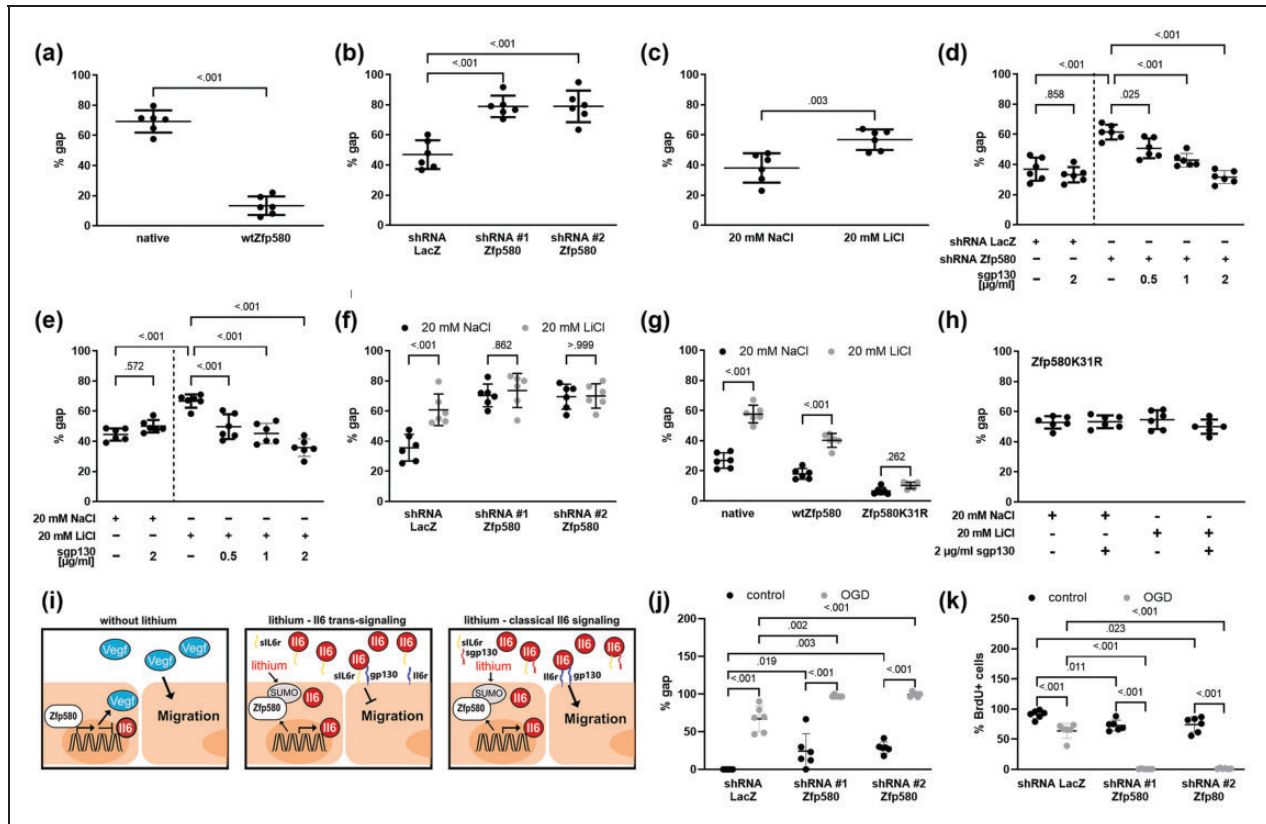


**Figure 3.** Effects of lithium and Zfp580 on endothelial cell migration and proliferation. Endothelial cell migration was determined using the scratch wound assay. Shown is the % of the remaining gap width after 24 h compared to the initial gap size. Increased expression of Zfp580 increased migration compared to that of native bEnd.3 cells (a) (two-tailed unpaired Student's *t*-test:  $t(10) = 14.18, p < .001$ ), and knockdown of Zfp580 reduced migration compared to that of bEnd.3 cells transfected with the LacZ control (b) (One-way ANOVA with Tukey's multiple comparison test:  $F(2, 15) = 24.5, p < .001$ ). Exposure to 20 mM LiCl reduced migration compared to that of control cells treated with 20 mM NaCl (c) (two-tailed unpaired Student's *t*-test:  $t(10) = 3.872, p = .003$ ). Blockade of *Il6* trans-signaling by the addition of 0.5 μg/ml, 1 μg/ml or 2 μg/ml sgp130 dose-dependently reduced the inhibitory effect of Zfp580 knockdown on endothelial cell migration (d) (One-way ANOVA with Tukey's multiple comparison test:  $F(5, 30) = 25.42, p < .001$ ) and reduced the inhibitory effect of 20 mM LiCl (e) (One-way ANOVA with Tukey's multiple comparison test:  $F(5, 30) = 18.94, p < .001$ ). This was not the case for shRNA LacZ-expressing or with 20 mM NaCl treated cells. Knockdown of Zfp580 completely abolished the effect of LiCl on endothelial cell migration (f) depending on knockdown, LiCl treatment and interaction between both factors ( $F(2, 15) = 19.22, p > .001$ ;  $F(1, 15) = 13.69, p = 0.002$ ;  $F(2, 15) = 8.971, p = .003$ ). The inhibitory effect of LiCl on endothelial cell migration was unchanged by increased expression of wild-type Zfp580, but this effect was completely blocked by expression of Zfp580K31R (g) depending on Zfp580 variant, LiCl treatment and interaction between both factors ( $F(2, 15) = 161.8, p < .001$ ;  $F(1, 15) = 249.49, p < .001$ ;  $F(2, 15) = 44.82, p < .001$ ). In Zfp580K31R, *Il6* trans-signaling inhibition by sgp130 showed no further effect on endothelial cell migration (h). (i) Illustration of the signaling. Without lithium, Zfp580 suppresses *Il6* expression. In the presence of lithium, Zfp580 is increasingly suppressed, SUMOylated and excluded from the nucleus. Therefore, *Il6* expression is disinhibited. In the presence of sll6r, *Il6* inhibits endothelial cell migration by *Il6* trans-signaling. After the addition of sgp130, *Il6* trans-signaling is inhibited, and classical *Il6* signaling enhances endothelial cell migration. (j) and (k) Cells were exposed to 4 h OGD directly after applying a scratch to the monolayer and incubated with BrdU. Migration (j) and proliferation (k) was determined 48 h later. Each, OGD and Zfp580 knock down reduced endothelial cell migration and proliferation. Combination of OGD and Zfp580 knock down almost completely prevented migration (Two-way ANOVA with Tukey's multiple comparison test: OGD  $F(1, 30) = 298.6, p < .001$ ; shRNA  $F(2, 30) = 22.73, p < .001$ ; interaction  $F(2, 30) = 0.1718, p = .843$ ) and proliferation (Two-way ANOVA with Tukey's multiple comparison test: OGD  $F(1, 30) = 397.0, p < .001$ ; shRNA  $F(2, 30) = 86.14, p < .001$ ; interaction  $F(2, 30) = 27.27, p < .001$ ). Graphs show scatter dot plots of the means of independent experiments  $\pm$  standard deviations.

### Zfp580 knock down strongly blocks endothelial cell migration and proliferation after OGD

We evaluated the role of Zfp580 in endothelial cell migration and proliferation after OGD, which is an

*in vitro* model of cerebral ischemia. Endothelial cells were exposed to 4 h of OGD and control group cells were cultured in OGD buffer with supplemental glucose and grown under normal oxygen conditions.

Migration was assessed by the scratch wound assay and proliferation by determining the percentage of BrdU positive cells. BrdU was applied on the cells directly after OGD. OGD significantly reduced endothelial cell migration (Figure 3(j)) and proliferation (Figure 3(k)). Zfp580 knock down reduced migration and proliferation even at control conditions. However, after OGD, Zfp580 knock down almost completely blocked migration and proliferation.

### ***Loss of Zfp580 improves survival of endothelial cells and neurons after OGD***

We then determined how Zfp580 is regulated under OGD in both, endothelial cells and neurons. Endothelial cells were exposed to 4 h of OGD and neurons to 2.5 h of OGD. In endothelial cells, Zfp580 mRNA was suppressed immediately after OGD, increased after 6 h, and then returned to baseline levels (Figure 4(a)). Zfp580 was regulated at the protein level in the same manner (Figure 4(b) and Supplemental Figure 3(g)). Il6 mRNA expression was inversely regulated (Figure 4(c)) and the induction of Il6 after OGD was significantly reduced when the non-SUMOylatable Zfp580K31R variant was expressed (Figure 4(d)). To evaluate the role of Zfp580 in cell survival after OGD, we determined the number of surviving cells after 4 h OGD. In LacZ-shRNA expressing endothelial cells, OGD induced a strong loss of endothelial cells whereas knock down of Zfp580 significantly improved endothelial cell survival (Figure 4(e)). In conclusion, inactivation of Zfp580 by degradation or SUMOylation after OGD induced Il6, and loss of Zfp580 improved endothelial cell survival after OGD.

In neurons, we measured Zfp580 protein levels by quantification of immunofluorescence staining (Figure 4(f) and (g)) and Zfp580 mRNA expression by real-time PCR (Figure 4(h)) after reoxygenation for different durations up to 24 h. At protein level, Zfp580 was suppressed in neurons immediately after OGD up to 24 h and at the mRNA level Zfp580 suppression began after 3 h of reoxygenation. We knocked down Zfp580 prior OGD, the neurons were subjected to 2.5 h of OGD and analyzed before and 24 h after OGD. Knock down of Zfp580 increased neuronal survival (Figure 4(i) and (j)). In addition, we determined the amount of released lactate dehydrogenase (LDH) as a marker of neuronal cell damage (Figure 4(k)). In the control group of LacZ-shRNA expressing neurons, we identified a strong increase of released LDH while there was no significant increase of LDH release when Zfp580 was knocked down. In contrast, expression of Zfp580K31R increased OGD-induced cell death of neurons (Figure 4(l)). Therefore, Zfp580 was rapidly suppressed after OGD in both principal cell-types of

the neurovascular unit and loss of Zfp580 was highly protective against OGD.

### ***Lithium improves neuronal survival after OGD only at toxic concentrations***

Then we determined the effect of lithium on neuronal survival after OGD. Treatment with 0.7 mM LiCl had no effect on neuronal cell death (Figure 4(m)), whereas treatment with 20 mM LiCl was significantly protective (Figure 4(n)). However, at this concentration, LiCl treatment was toxic under control conditions. In contrast, Zfp580 knock down showed no toxic effects in neurons (Figure 4(j) and (k)). Therefore, Zfp580 inhibition might be a more promising target for stroke treatment than LiCl treatment. In the following *in vivo* experiments, we focused on Zfp580.

### ***Zfp580 is ubiquitously expressed throughout the brain in neurons and vessels, and genomic ablation has no effect on cognitive or motor function***

We investigated whether Zfp580 is expressed in the brain by staining brain sections from C57BL/6 mice for Zfp580. Zfp580 expression was found throughout the brain, particularly in neurons and blood vessels. (Figure 5(a)). We used the Zfp580tm1a<sup>(EUCOMM)Wtsi</sup> constitutive knockout mouse model from the EUCOMM project for further experiments. In Zfp580tm1a mice, no Zfp580 signal was detectable by immunofluorescence (Figure 5(b)). To determine whether Zfp580 affects basal neuronal functions, we tested Zfp580tm1a with behavioral tests for cognitive and motor functions. Zfp580 knockout had no effect on cognitive tests such as the novel object recognition test (Figure 5(c) to (e)) and the Y-maze test (Figure 5(g) and (h)), nor on motor tests such as the Rotarod test (Figure 5(f)) and the Staircase test of skilled pellet-reaching (Figure 5(i) and (j)). Therefore, Zfp580 knockout mice showed no behavioral alterations compared to wild-type mice and Zfp580 knockout had no confounding effect on cognitive or motor behavioral tests.

### ***Genomic ablation of Zfp580 reduces the chronic ischemic lesion size***

Next, we evaluated the effects of Zfp580 knockout on ischemic lesion size. Zfp580 knockout mice and wild-type littermates underwent transient 45-min filamentous occlusion of the middle cerebral artery. We determined the ischemic lesion size one day after stroke using T2-weighted MRI sequences and correlated the detected lesion to anatomical regions using the Allen brain atlas using our custom-made algorithm (Figure 6(a)).<sup>29</sup> After transient filamentous MCAo,

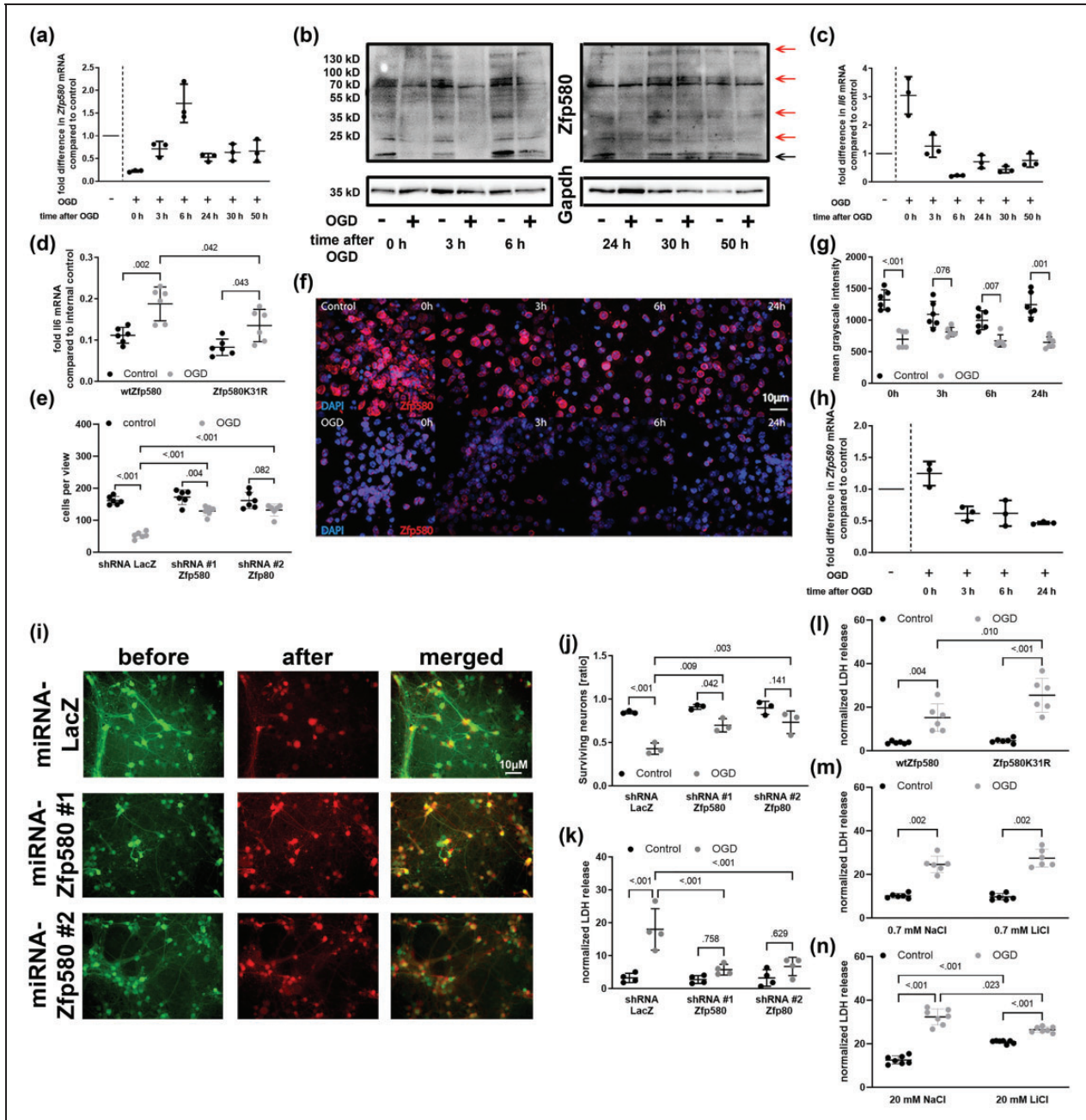


**Figure 4.** OGD induces Il6 via Zfp580 suppression and inactivation, and Zfp580 loss improves endothelial and neuronal survival after OGD. Stroke was simulated *in vitro* by oxygen and glucose deprivation (OGD) for 4 h in endothelial cells ((a) – (e)) and for 2.5 h in neurons ((f) – (n)). Cells cultured under normal oxygen and glucose levels served as negative controls. Samples were taken after reoxygenation for several periods after OGD, as indicated in the figure. (a) Real-time RT-PCR for Zfp580 mRNA. In endothelial cells, mRNA expression of Zfp580 was immediately suppressed after OGD, increased after 6 h of reoxygenation and restored to baseline thereafter (descriptive results,  $n = 3$ ). (b) Immunoblot for the Zfp580 protein. Zfp580 protein expression was regulated in a manner similar to that of Zfp580 mRNA expression. (c) Il6 mRNA was inversely regulated after OGD (descriptive results,  $n = 3$ ). (d) Increased expression of wtZfp580 failed to block Il6 mRNA induction after OGD, whereas expression of SUMO conjugation-resistant Zfp580K31R significantly reduced Il6 mRNA induction compared to wtZfp580 (Two-way ANOVA with Tukey's multiple comparison test: OGD  $F(1, 20) = 24.82, p < .001$ ; Zfp580 variant  $F(1, 20) = 10.03, p = 0.005$ ; interaction  $F(1, 20) = 0.833, p = .372$ ). (e) Number of surviving endothelial cells 48 h after 4 h OGD. OGD caused cell loss and knock down of Zfp580 significantly increased the number of surviving cells (Two-way ANOVA with Tukey's multiple comparison test: OGD  $F(1, 30) = 97.14, p < .001$ ; shRNA  $F(2, 30) = 20.27, p < 0.001$ ; interaction  $F(2, 30) = 15.42, p < .001$ ). (f) and (g). In neurons, quantification of immunofluorescence staining for Zfp580 showed an immediate loss of Zfp580 protein levels after OGD (Two-way RM ANOVA with Sidak's multiple comparison test: OGD  $F(1, 10) = 113.9, p < .001$ ; time  $F(2.321, 23.21) = 3.022, p = 0.061$ ; interaction  $F(3, 30) = 4.565, p = .009$ ). (h) The mRNA expression of

Continued.



lesions beyond the territory of the middle cerebral artery can occur as a technical failure caused by random additional occlusion of the posterior communicating artery and the high variability of the circle of Willis in C56BL/6 mice. The presence of lesions beyond the middle cerebral artery territory is especially sensitive to the presence or absence of the P1 segment of the posterior cerebral artery.<sup>35</sup> Lesions in the posterior territory, such as the visual cortex or hippocampal formation, strongly affect behavioral testing. Therefore, mice with ischemic lesions beyond the territory of the middle cerebral artery were excluded to avoid a bias in lesion size and behavioral testing. One day after ischemia, we observed a trend toward smaller lesion size on MRI (Figure 6(a) and (b)). After 21 days, the lesion size was determined histologically by NeuN staining. At this time point, the histological lesion size in the Zfp850 knockout mice was significantly smaller than in wild-type littermates (Figure 6(c)). Therefore, Zfp580 knockout was neuroprotective *in vivo* and reduced ischemic lesion size in the long-term.

#### **Zfp580 knockout reduced endothelial cell proliferation but increased vessel resilience to ischemia**

To examine the effects of Zfp580 knockout on post-ischemic angiogenesis, the mice received intraperitoneal BrdU injections from day two to five after MCAo. We stained brain sections 21 days after MCAo for Caveolin-1 and BrdU to visualize endothelial cells and to identify proliferating endothelial cells. Figure 6(d) shows stainings within the ischemic area, Figure 6(e) the quantification of Caveolin-1/BrdU double positive cells, Figure 6(f) the quantification of vessel density and Figure 6(g) the area covered by Caveolin-1 positive vessels (vessel area). The number of proliferating endothelial cells was reduced in Zfp580 knockout mice. However, vessel density and vessel area were higher in Zfp580 knockout mice. Overall, even though Zfp580 knockout decreased angiogenic mechanisms like endothelial cell proliferation, it appeared protective for blood

vessels after stroke, resulting in enhanced vascularization of the ischemic region.

#### **Genomic ablation of Zfp580 modulates paracrine Il6 signaling**

To evaluate the effects of Zfp580 knockout on Il6 signaling after stroke, we determined local paracrine cerebral *Il6* mRNA expression two days after ischemia by real-time RT-PCR (Figure 6(h)). We separated the ipsilesional and contralesional hemispheres using 2-mm brain slices within the infarcted area. There was no difference in Il6 expression between the ipsilesional and contralesional hemispheres in sham-operated mice of both genotypes. In wild-type mice, we observed an increase in *Il6* expression in the ipsilesional hemisphere after stroke. In Zfp580 knockout mice, *Il6* induction was less pronounced. To examine the effects of Zfp580 knockout on systemic Il6 responses and Il6 trans-signaling, we determined Il6 and sIl6r levels in the blood by ELISA two days after stroke (Figure 6(i) and (j)). There was no difference in Il6 levels between genotypes. Blood sIl6r levels were higher in Zfp580 knockout mice than in wild-type littermates. In addition, we calculated the Il6:sIl6r binary complex, which reflects the amount of Il6 trans-signaling (Figure 6(k)). In Zfp580 knockout mice, the Il6:sIl6r binary complex was also higher than in wild-type littermates, indicating increased Il6 trans-signaling. These findings suggest that Zfp580 knockout decreases paracrine cerebral Il6 responses, but increases cerebral and systemic Il6 trans-signaling following stroke.

#### **Zfp580 knockout modulates cerebral connectivity after stroke**

We studied changes in neuronal connectivity induced by Zfp580 knockout 21 days after stroke using diffusion MRI. In an exploratory, unbiased approach, we used a map of 154 nodes per hemisphere representing functional anatomical regions correlated with the Allen Brain Atlas, resulting in 23,562 possible connections.

#### **Figure 4. Continued.**

Zfp580 was immediately suppressed up to 24 h after OGD (descriptive results,  $n = 3$ ). ((i) – (k) Neurons were subjected to 2.5 h OGD. Images were taken before and 24 h after OGD at identical positions (i). The number of surviving cells was counted (j) and the released LDH was determined from the cell culture supernatants (k). Knockdown of Zfp580 prior OGD increased the number of surviving cells (Two-way ANOVA with Tukey's multiple comparison test: OGD  $F(1, 12) = 56.51$ ,  $p < .001$ ; shRNA  $F(2, 12) = 10.49$ ,  $p = 0.002$ ; interaction  $F(2, 12) = 4.791$ ,  $p = .03$ ) and reduced the LDH release (Two-way ANOVA with Tukey's multiple comparison test: OGD  $F(1, 18) = 30.32$ ,  $p < .001$ ; shRNA  $F(2, 18) = 9.804$ ,  $p = 0.001$ ; interaction  $F(2, 18) = 8.931$ ,  $p = .002$ ). (l) Expression of the non-SUMOylatable Zfp580K31R variant increased the LDH release after OGD compared to the wild-type variant (Two-way ANOVA with Tukey's multiple comparison test: OGD  $F(1, 20) = 61.22$ ,  $p < .001$ ; shRNA  $F(1, 20) = 7.245$ ,  $p = 0.014$ ; interaction  $F(1, 20) = 5.307$ ,  $p = .032$ ). (m) Treatment with 0.7 mM LiCl had no effect on neuronal LDH release. (n) Treatment with 20 mM LiCl significantly reduced LDH release, but LiCl was toxic at control conditions (Two-way RM ANOVA with Sidak's multiple comparison test: OGD  $F(1, 6) = 155.1$ ,  $p < .001$ ; LiCl  $F(1, 6) = 5.28$ ,  $p = 0.061$ ; interaction  $F(1, 6) = 48.58$ ,  $p < .001$ ). Graphs show scatter dot plots of the means of independent experiments  $\pm$  standard deviation.

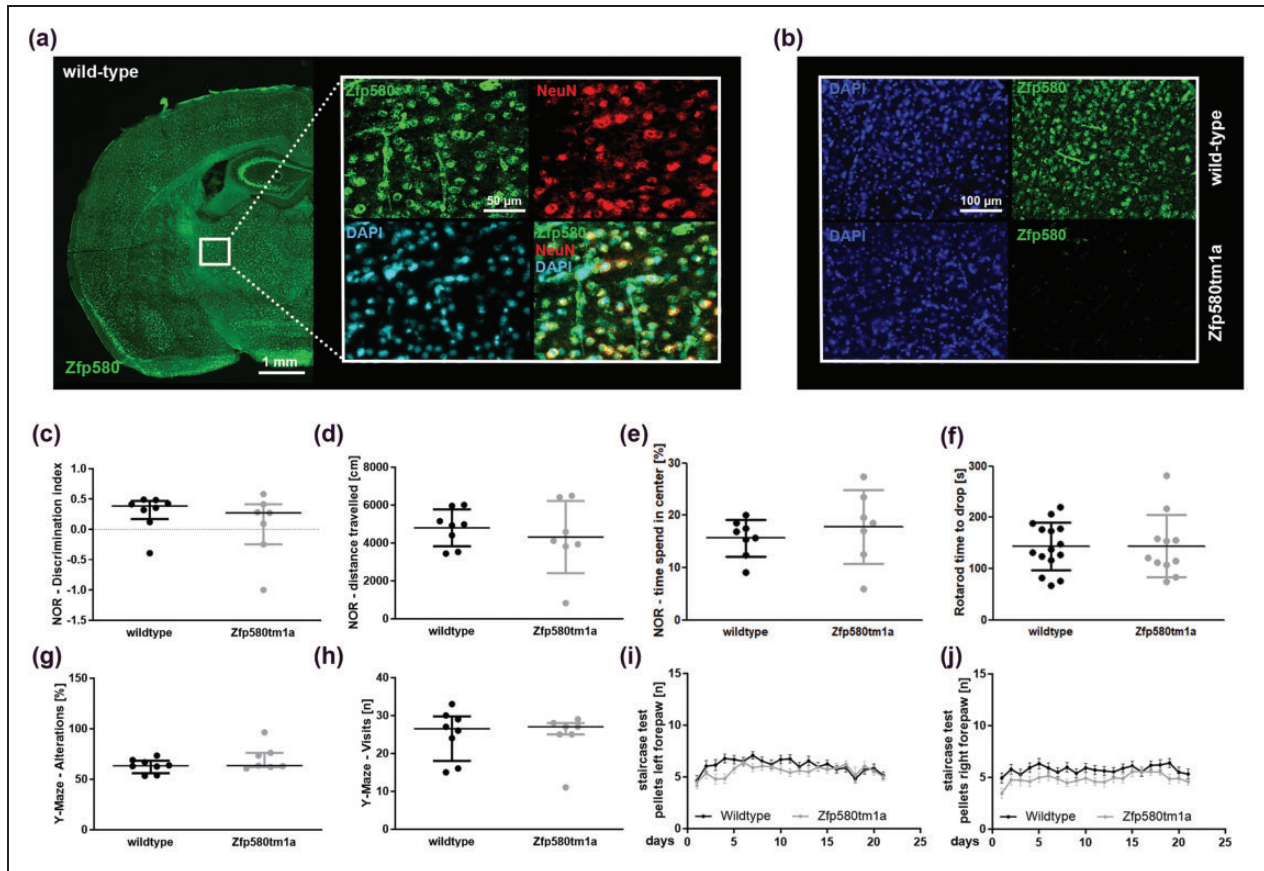


**Figure 5.** Zfp580 is ubiquitously expressed throughout the brain in neurons and vessels, and genomic ablation has no effect on cognitive or motor function. (a) Zfp580, NeuN, and DAPI immunofluorescence staining of C57BL/6 mouse brain slices. Zfp580 expression was found throughout the brain, particularly in neurons and blood vessels. (b) In Zfp580tm1a mice, no Zfp580 signal was detectable by immunofluorescence. Genomic ablation of Zfp580 had no biasing effect on the performance of mice in the Novel object recognition test (c)–(e), Rotarod test (f), Y-Maze test (g) and (h) or Staircase test (i) and (j). Graphs show scatter dot plots of the means of independent experiments  $\pm$  standard deviations ((d)–(f), (i) and (j)), median  $\pm$  interquartile range ((c), (g) and (h)).

Using the T-statistic with  $p < 0.001$ , 23 connections were significantly altered. Of these, 11 connections were increased (Figure 7(a)) and 12 connections were decreased (Figure 7(b)). Most connectivity changes were observed in the contralesional hemisphere. The connectivity changes converged in specific areas. The contralesional ride-sided external segment of the globus pallidus showed increased connectivity to the right-sided ectorhinal area and lateral septal nucleus and to the left-sided prelimbic area. Another focus on connectivity changes was noted in the dorsal part of the right-sided contralesional retrosplenial area with increased connectivity to the right-sided pontine and midbrain reticular nuclei. Moreover, this area showed increased connectivity to the left-sided cerebellar culmen. In contrast, on the left side, this area showed decreased connectivity to the left-sided anterior cingulate area and orbital area. We identified the right-sided posterolateral visual area as the focus for the decreased

connectivity. This area showed decreased connectivity with the cerebellar simple lobule and crus 1 on the right side and with the right parasubiculum. Additionally, the right-sided primary visual area showed decreased connectivity to the right-sided cerebellar simple lobule, whereas connectivity within the visual area on the right side increased (rostromedial visual area and anteromedial visual area). On the right side, the dentate gyrus showed reduced connectivity with the colliculus superior, the geniculate group of the ventral thalamus and the lateral zone of the hypothalamus. In conclusion, the connectivity changes we observed mostly affected visuospatial motor and motivational functions of the contralesional hemisphere.

#### *Zfp580 knockout improves functional recovery*

Functional outcome was assessed using the modified DeSimoni Neuroscore as an overall disease score and the Rotarod test as a test of gross motor function at

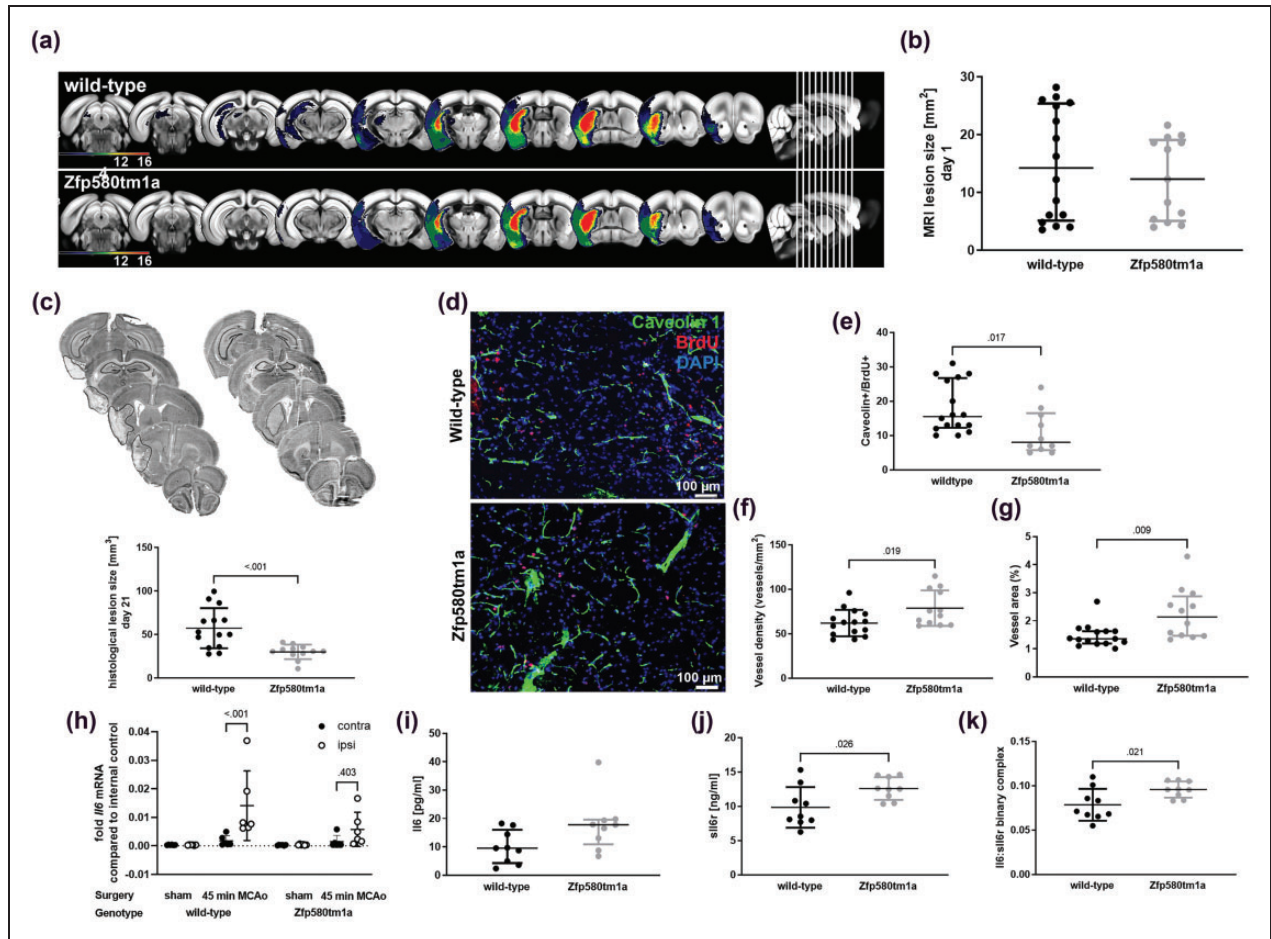


**Figure 6.** Genomic ablation of *Zfp580* reduces ischemic lesion size, reduces endothelial proliferation, increases vessel resilience to ischemia, and modulates paracrine *Il6* responses. Mice underwent transient filamentous occlusion of the middle cerebral artery for 45 min. (a) and (b) Lesion size was determined by MRI one day after ischemia and correlated to anatomical regions. The following mice were excluded from further analysis: mice without stroke, mice with stroke beyond the territory of the middle cerebral artery, and mice that reached predetermined humane endpoints and were therefore euthanized. There was no difference in lesion size one day after ischemia (Mann-Whitney test:  $p = .531$ ). (c) Histological quantification of NeuN-DAB staining 21 days after ischemia revealed smaller lesion size in the *Zfp580* knockout mice (two-tailed unpaired Student's *t*-test with Welch's correction:  $t(16.80) = 4.120$ ,  $p < .001$ ). (d) Caveolin-1, BrdU and DAPI staining of endothelial cells in the ischemic area of *Zfp580* knockout mice and wild-type littermates 21 days after stroke. BrdU was administered from day two to five. (e) The amount of proliferating endothelial cells (Caveolin+/BrdU+ cells) was reduced in *Zfp580tm1a* in the ischemic area (Mann-Whitney test:  $p = .017$ ). (f) Vessel density (two-tailed unpaired Student's *t*-test:  $t(25) = 2.501$ ,  $p < .019$ ) and (g) Caveolin-1-positive vessel area (Mann-Whitney test:  $p = .009$ ) were increased in *Zfp580* knockout mice compared to wild-type littermates. (h) Real-time RT-PCR was performed from ipsilesional and contralesional brain slices taken from within the infarcted area 2 days after stroke. *Il6* was strongly induced in the ipsilesional hemisphere in wild-type littermates, while *Il6* induction was less pronounced in *Zfp580* knockout mice (Two-way RM ANOVA with Sidak's multiple comparison test: hemisphere  $F(1, 20) = 9.959$ ,  $p = .005$ ; treatment  $F(3, 20) = 5.706$ ,  $p = 0.005$ ; interaction  $F(3, 20) = 4.807$ ,  $p = .011$ ). ELISA for *Il6* (i) and *sll6r* (j) was performed from blood samples 2 days after stroke. (i) There was no difference in *Il6* levels between genotypes (Mann-Whitney test:  $p = .063$ ). (j) In *Zfp580* knockout mice, *sll6r* blood levels were higher than those in wild-type littermates (two-tailed unpaired Student's *t*-test:  $t(16) = 2.444$ ,  $p = .026$ ) and (k) Calculated *Il6*:*sll6r* binary complex. In *Zfp580* knockout mice, *Il6* trans-signaling was increased (two-tailed unpaired Student's *t*-test:  $t(16) = 2.565$ ,  $p = .021$ ). Graphs show scatter dot plots of data from independent mice or samples derived thereof  $\pm$  standard deviations ((c), (f), (h), (j) and (k)) or median  $\pm$  interquartile range ((b), (e), (g) and (i)).

2, 7 and 14 days after ischemia. The staircase test of sucrose-pellet reaching was conducted daily to assess the side-specific fine motor function of the forepaws. Visual-spatial motor functions are highly relevant for the staircase test. We did not detect a difference in the

modified DeSimoni Neuroscore between genotypes at any time point (Figure 7(c)). However, *Zfp580* knockout mice fared significantly better than wild-type littermates in the Rotarod test (Figure 7(d)). In the staircase test, motor function of the right forepaw recovered



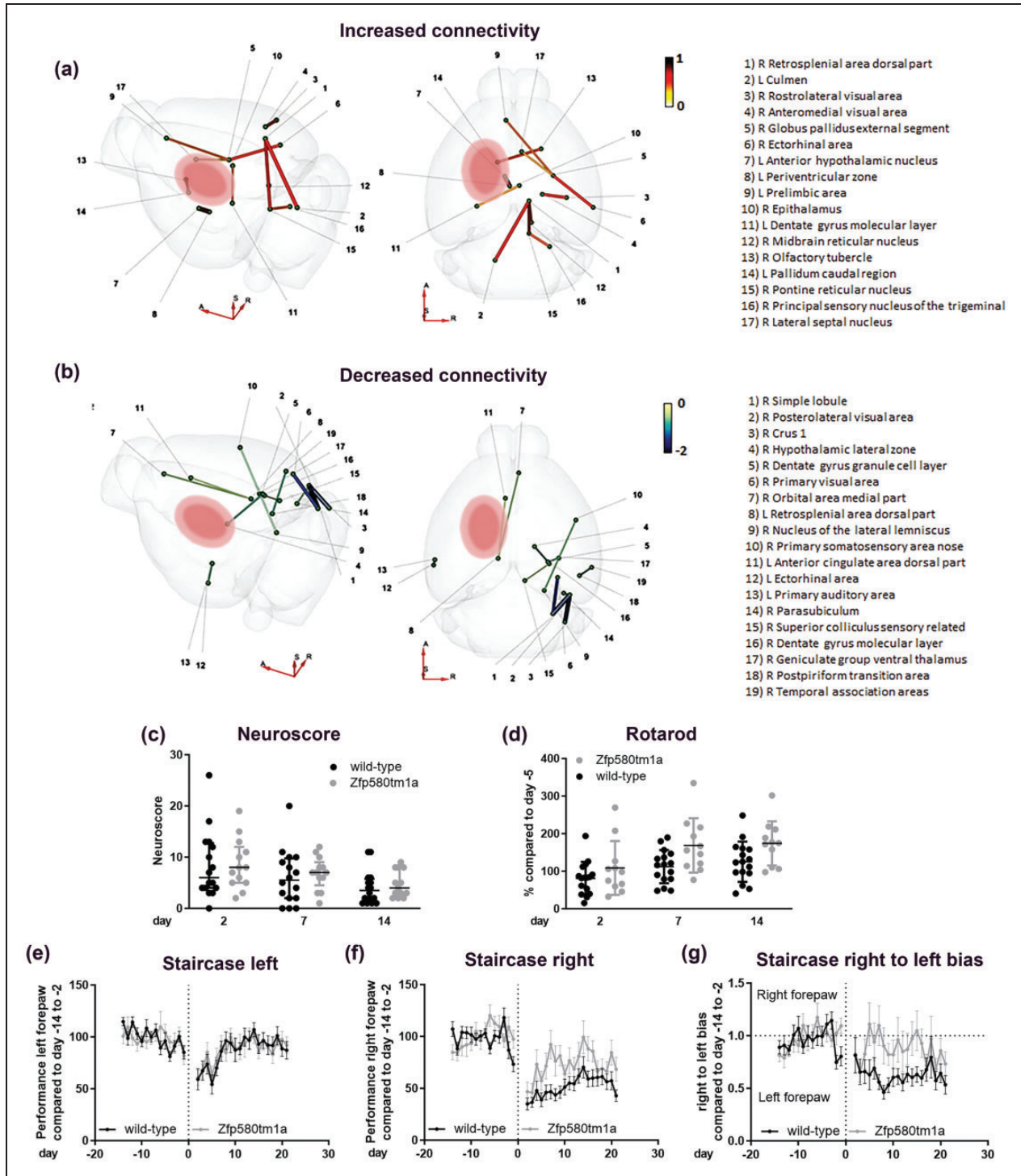


**Figure 7.** Zfp580 knockout modulates cerebral connectivity and improves functional recovery after stroke. (a) and (b) Connectivity was determined 21 days after MCAo using diffusion tensor imaging. The connection strength of Zfp580 knockout mice compared to wild-type littermates is displayed using T-statistics with  $p < .001$  chosen as relevant. (a) An increase of connection strength was observed in 11 connections with a focus on the contralesional external segment of the globus pallidus and the dorsal part of the contralesional retrosplenial area. (b) A decrease of connection strength was observed in 12 connections with a focus on the contralesional posterolateral visual area and contralesional dentate gyrus. Functional recovery of these mice was determined by behavioral tests. (c) There was no difference in the modified DeSimoni Neuroscore (Two-way RM ANOVA with Sidak's multiple comparison test: genotype  $F(1, 27) = 0.1516$ ,  $p = .7$ ; time  $F(1.716, 46.32) = 14.41$ ,  $p < 0.001$ ; interaction  $F(2, 54) = 0.075$ ,  $p = 928$ ). Zfp580 knockout mice performed better in the Rotarod test (d) (Two-way RM ANOVA with Sidak's multiple comparison test: genotype  $F(1, 25) = 4.807$ ,  $p = .038$ ; time  $F(1.605, 40.11) = 28.33$ ,  $p < 0.001$ ; interaction  $F(2, 50) = 1.849$ ,  $p = .168$ ). (e) There was no

Continued.

faster and to a greater extent in Zfp580 knockout mice (Figure 7(f)). There was no difference in left forepaw performance between Zfp580 knockout mice and wild-type littermates (Figure 7(e)). Moreover, Zfp580 knockout mice used the right forepaw more frequently than wild-type littermates (Figure 7(g)). Therefore, Zfp580 knockout improved sensori-motor function outcome after stroke.

## Discussion

In this study we identified Zfp580 inhibition as a new treatment strategy to improve stroke outcome. Previous studies suggested that lithium treatment might be an option to improve stroke outcome, however, lithium might have serious side effects. Here, we showed that Zfp580 mediates lithium's effects on Il6 signaling. In contrast to lithium, Zfp580 inhibition showed no neurotoxicity and Zfp580 knockout mice showed no obvious phenotypic alterations. We identified SUMOylation as new mechanism that modulates Zfp580 functions. Loss of Zfp580 was highly neuroprotective, increased endothelial cell resilience to ischemia, modulated paracrine cerebral Il6 signaling, and enhanced use-dependent neuroplasticity.

Zfp580 acted as an inhibitor of Il6. *In vivo*, Il6 expression was comparable between Zfp580 knockout mice and wild-type littermates. Thus, Zfp580 knockout did not modulate basal levels of Il6. We discovered a previously unknown SUMOylation site of Zfp580 at the lysine residue at position 31. Lithium specifically induced Zfp580 SUMOylation without enhancing global SUMOylation of proteins. Mono-SUMOylated Zfp580 was in the nucleus, while poly-SUMOylation of Zfp580 led to its exclusion from the nucleus, a very common effect of transcription factor SUMOylation.<sup>36</sup> Zfp580 SUMOylation was essential to inactivate Zfp580.

Lithium and Zfp580 knock down reduced migration of endothelial cells. This was surprising, since both induced Il6, which is believed to enhance migration and proliferation by classical Il6 signaling.<sup>37</sup> We showed that in contrast to classical Il6 signaling, Il6 trans-signaling inhibits endothelial cell migration. When we blocked the inactivation of Zfp580 by mutating the SUMOylation site (K31R), migration was

pronounced and lithium had no effect on migration. Thus, we have identified a completely new pathway that mediates the effects of lithium on endothelial cell migration.

We have found that Zfp580 protein is ubiquitously highly expressed in neurons in the brain. A recent study showed, that Zfp580 is induced in a neonatal hypoxic-ischemic brain damage model of rats and that it is protective in the human neuroblastoma cell line SH-SY5Y after OGD.<sup>23</sup> Surprisingly, we found the opposite results: *In vitro* after OGD, Zfp580 was rapidly and transiently reduced in endothelial cells and primary neuronal cultures. Knockdown of Zfp580 was highly neuroprotective and increased endothelial cell survival after OGD and Zfp580 knockout reduced ischemic lesion size over the long term. These conflicting results could be explained by different regulations and functions of Zfp580 in endothelial cells and primary neuronal cultures compared to a cell line derived from a neuroblastoma such as SH-SY5Y. Zfp580 might have different *in vivo* effects in neonatal hypoxia than in a stroke. Interestingly, acutely after stroke, we found no difference in ischemic lesion size between genotypes, but in the long-term. This might point towards a prolonged neuroprotective effect of Zfp580 knockout.

After stroke, Il6 was locally induced in the ischemic tissue, but Il6 induction was less pronounced in Zfp580 knockout mice. Therefore, postischemic Zfp580 loss partially mediated the effects of stroke on Il6 expression. However, Zfp580 knockout led to increased sIl6r levels. This resulted in increased Il6 trans-signaling in Zfp580 knockout mice during the acute phase of stroke, whereas classical signaling appears to have been more prominent in wild-type littermates. Pronounced Il6 trans-signaling in Zfp580 knockout mice may reduce endothelial cell migration. Furthermore, we observed reduced endothelial cell proliferation *in vitro* after Zfp580 knock down and in Zfp580 knock out mice after stroke, indicating reduced angiogenesis. However, the vessel density in the ischemic area was higher in Zfp580 knockout mice 21 days after ischemia. *In vitro*, we observed an increased survival of endothelial cells after OGD, when Zfp580 was knocked down. Therefore, the increase in vessel density might be explained by an improved survival of endothelial cells after stroke.

### Figure 7. Continued.

difference in performance of the left forepaw in the staircase test between genotypes (Two-way RM ANOVA with Sidak's multiple comparison test: genotype  $F(1, 27) = 0.001$ ,  $p = .97$ ; time  $F(9.616, 259.6) = 5.144$ ,  $p < 0.001$ ; interaction  $F(33, 891) = 0.6454$ ,  $p = .94$ ). (f) The performance of the right forepaw recovered better in Zfp580 knockout mice (Two-way RM ANOVA with Sidak's multiple comparison test: genotype  $F(1, 27) = 5.825$ ,  $p = .023$ ; time  $F(8.761, 236.5) = 13.87$ ,  $p < 0.001$ ; interaction  $F(33, 891) = 2.285$ ,  $p < .001$ ) and (g) Zfp850-knockout mice used the right forepaw more than wild-type littermates (Two-way RM ANOVA with Sidak's multiple comparison test: genotype  $F(1, 27) = 7.499$ ,  $p = .011$ ; time  $F(10.80, 291.7) = 2.947$ ,  $p = 0.001$ ; interaction  $F(33, 891) = 1.536$ ,  $p = .028$ ). Graphs show scatter dot plots of data from independent mice or samples derived thereof  $\pm$  standard deviations.

Zfp580 knockout modulated the cerebral connectivity after stroke. Overall, Zfp580 knockout affected connections relevant for visuospatial and motivational functions, mostly in the contralesional hemisphere. In detail, connectivity was changed to the retrosplenial area, which is relevant to spatial cognition,<sup>38</sup> to the rostralateral visual area and anteromedial visual area, which both processes motion information,<sup>39</sup> to the contralesional primary visual area and posterolateral visual area, and to the contralesional ride-sided external segment of the globus pallidus, which is involved in control of motor functions. Connectivity was changed to the lateral septal nucleus as a central regulator of emotional, motivational and spatial behavior,<sup>40</sup> and to the prelimbic area, which is needed for strategy and attentional set shifting and modulation of attention towards predictive stimuli.<sup>41</sup> In the end, Zfp580 knockout led to improved outcomes regarding gross motor function in the Rotarod test and fine motor skills of the paretic right forepaw in the staircase test. Interestingly, visuospatial and motivational functions are highly relevant for these tests and, therefore, the mice were regularly trained in these functions by the daily stair case testing. Hence, the changes in connectivity we observed might indicate that Zfp580 knockout enhanced use-dependent neuroplasticity in response to the staircase test.

The major limitation of this study is that we provide preclinical evidence in a constitutive knockout mouse model. Further research is needed to evaluate which cell types are responsible for the shown effects of Zfp580 on stroke recovery. We continue to pursue this question using cell-type specific conditional knockout mice, which we recently generated. Furthermore, although we showed the effects of Zfp580 on Il6 signaling *in vitro* and *in vivo* and the beneficial effects of Zfp580 knockout on recovery after stroke, we did not directly prove the causal relationship between Zfp580-dependent Il6 signaling modulation and stroke recovery. However, in our previous work we already showed strong evidence that Il6 signaling has a strong impact on stroke recovery and neuronal network remodeling.<sup>1,7,42</sup> We focused on the effects of Zfp580 on Il6. Studying the effects on other cytokines might be interesting for future studies.

In conclusion, we have identified inhibition of Zfp580 as a novel potential therapeutic strategy to reduce infarct size, preserve vascularization of the ischemic area, modulate postischemic paracrine cerebral Il6 responses and trans-signaling, and enhance use-dependent neuroplasticity to foster recovery after stroke. Inactivation of Zfp580 acts down-stream of lithium and acts positively on several key mechanisms without showing relevant adverse side effects compared to lithium, making it possibly a more specific and

effective treatment target. Development of Zfp580 inhibitors is required to further evaluate its potential.

### Funding

The author(s) disclosed receipt of the following financial support for the research, authorship, and/or publication of this article: Funding was provided by the Deutsche Forschungsgemeinschaft (DFG, German Research Foundation) to C.J.H. and C.H. (Project-ID 417284923) and Collaborative Research Center ReTune TRR 295- Project-ID 424778381 to C.H. and M.E.; Einstein Centre of Regenerative Therapies (Einstein Kickbox starting grant to C.J.H.); and German Federal Ministry of Education and Research (BMBF CSB 01EO1301) to C.H. and M.E. C.J.H. and L.K. are participants in the Charité Clinical Scientist Program funded by the Charité-Universitätsmedizin Berlin and the Berlin Institute of Health. M.K. received funding from the Graduate School 203 of the DFG Excellence Initiative, Berlin-Brandenburg School for Regenerative Therapies. L.S.F. acknowledges the support of the Cluster of Excellence Matters of Activity. Image Space Material funded by the Deutsche Forschungsgemeinschaft (DFG, German Research Foundation) under Germany's Excellence Strategy—EXC 2025—390648296. M.E. received funding from DFG under Germany's Excellence Strategy – EXC-2049 – 390688087, BMBF, DZNE, DZHK, EU, Corona Foundation, and Fondation Leducq to ME and CH. Funding to S.M., S.P.K. and P.B.S. was provided by the BMBF under the ERA-NET NEURON scheme (01EW1811) and the DFG (Project-ID 428869206). Noninvasive MRI measurements allowed a longitudinal study design and were supported by Charité 3R, Replace – Reduce – Refine.

### Acknowledgements

We greatly acknowledge expert advice and generous support of Ulrich Dirnagl. Technical assistance by Monica Dopatka and Marco Foddis is greatly acknowledged.

### Declaration of conflicting interests

The author(s) declared no potential conflicts of interest with respect to the research, authorship, and/or publication of this article.


### Authors' contributions

Study conception and design: C.J.H., M.E. and C.H. Conducting experiments, data collection and analysis: C.J.H., M.K. S.L., L.K., J.L., P.B.S., S.M., S.P.K., J.A., L.S.F., P.B., A.R., G.L., M.E. and C.H. All authors read and approved the final manuscript.


### ORCID iDs

Christian J Hoffmann  <https://orcid.org/0000-0003-0861-2418>

Leif Koschützke  <https://orcid.org/0000-0002-3709-5598>

Philipp Boehm-Sturm  <https://orcid.org/0000-0001-8777-4823>

Jeehye An  <https://orcid.org/0000-0002-3812-2420>

Christoph Harms  <https://orcid.org/0000-0002-2063-2860>



## Supplemental material

Supplemental material for this article is available online.

## References

- Gertz K, Kronenberg G, Kalin RE, et al. Essential role of interleukin-6 in post-stroke angiogenesis. *Brain* 2012; 135: 1964–1980.
- Suzuki S, Tanaka K and Suzuki N. Ambivalent aspects of interleukin-6 in cerebral ischemia: inflammatory versus neurotrophic aspects. *J Cereb Blood Flow Metab* 2009; 29: 464–479.
- Hunter CA and Jones SA. IL-6 as a keystone cytokine in health and disease. *Nat Immunol* 2015; 16: 448–457.
- Rose-John S. The soluble interleukin 6 receptor: Advanced therapeutic options in inflammation. *Clin Pharmacol Ther* 2017; 102: 591–598.
- Leibinger M, Zeitler C, Gobrecht P, et al. Transneuronal delivery of hyper-interleukin-6 enables functional recovery after severe spinal cord injury in mice. *Nat Commun* 2021; 12: 391.
- Willis EF, MacDonald KPA, Nguyen QH, et al. Repopulating microglia promote brain repair in an IL-6-Dependent manner. *Cell* 2020; 180: 833–846 e16.
- Hoffmann CJ, Harms U, Rex A, et al. Vascular signal transducer and activator of transcription-3 promotes angiogenesis and neuroplasticity long-term after stroke. *Circulation* 2015; 131: 1772–1782.
- Bustamante A, Sobrino T, Giralt D, et al. Prognostic value of blood interleukin-6 in the prediction of functional outcome after stroke: a systematic review and meta-analysis. *J Neuroimmunol* 2014; 274: 215–224.
- Boufidou F, Nikolaou C, Alevizos B, et al. Cytokine production in bipolar affective disorder patients under lithium treatment. *J Affect Disord* 2004; 82: 309–313.
- Rapaport MH, Guylai L and Whybrow P. Immune parameters in rapid cycling bipolar patients before and after lithium treatment. *J Psychiatr Res* 1999; 33: 335–340.
- Kim YR, van Meer MP, Tejima E, et al. Functional MRI of delayed chronic lithium treatment in rat focal cerebral ischemia. *Stroke* 2008; 39: 439–447.
- Mohammadianinejad SE, Majdinasab N, Sajedi SA, et al. The effect of lithium in post-stroke motor recovery: a double-blind, placebo-controlled, randomized clinical trial. *Clin Neuropharmacol* 2014; 37: 73–78.
- Guo S, Arai K, Stins MF, et al. Lithium upregulates vascular endothelial growth factor in brain endothelial cells and astrocytes. *Stroke* 2009; 40: 652–655.
- Mao CD, Hoang P and DiCorleto PE. Lithium inhibits cell cycle progression and induces stabilization of p53 in bovine aortic endothelial cells. *J Biol Chem* 2001; 276: 26180–26188.
- Struewing IT, Durham SN, Barnett CD, et al. Enhanced endothelial cell senescence by lithium-induced matrix metalloproteinase-1 expression. *J Biol Chem* 2009; 284: 17595–17606.
- Zeilbeck LF, Muller B, Knobloch V, et al. Differential angiogenic properties of lithium chloride in vitro and in vivo. *PLoS One* 2014; 9: e95546.
- Hoffmann CJ, Hohberg M, Chlench S, et al. Suppression of zinc finger protein 580 by high oxLDL/LDL-ratios is followed by enhanced expression of endothelial IL-8. *Atherosclerosis* 2011; 216: 103–108.
- Stenzel P, Nagorsen K, Bernd J, et al. ZNF580 – a brake on interleukin-6. *J Inflamm (Lond)* 2018; 15: 20.
- Luo Y, Zhao Y, Li X, et al. ZNF580 mediates eNOS expression and endothelial cell migration/proliferation via the TGF-beta1/ALK5/Smad2 pathway. *Mol Cell Biochem* 2014; 393: 199–207.
- Shi C, Yao F, Li Q, et al. Regulation of the endothelialization by human vascular endothelial cells by ZNF580 gene complexed with biodegradable microparticles. *Biomaterials* 2014; 35: 7133–7145.
- Sun HY, Wei SP, Xu RC, et al. Sphingosine-1-phosphate induces human endothelial VEGF and MMP-2 production via transcription factor ZNF580: novel insights into angiogenesis. *Biochem Biophys Res Commun* 2010; 395: 361–366.
- Meng XY, Yu HL, Zhang WC, et al. ZFP580, a novel zinc-finger transcription factor, is involved in cardioprotection of intermittent high-altitude hypoxia against myocardial ischemia-reperfusion injury. *PLoS One* 2014; 9: e94635.
- Yin C, Ji Y, Ma N, et al. RNA-seq analysis reveals potential molecular mechanisms of ZNF580/ZFP580 promoting neuronal survival and inhibiting apoptosis after hypoxic-ischemic brain damage. *Neuroscience* 2022; 483: 52–65.
- Datwyler AL, Lattig-Tunneemann G, Yang W, et al. SUMO2/3 conjugation is an endogenous neuroprotective mechanism. *J Cereb Blood Flow Metab* 2011; 31: 2152–2159.
- Ziegler L, Gajulapuri A, Frumento P, et al. Interleukin 6 trans-signalling and risk of future cardiovascular events. *Cardiovasc Res* 2019; 115: 213–221.
- Harms C, Albrecht K, Harms U, et al. Phosphatidylinositol 3-Akt-kinase-dependent phosphorylation of p21(Waf1/Cip1) as a novel mechanism of neuroprotection by glucocorticoids. *J Neurosci* 2007; 27: 4562–4571.
- Freyer D and Harms C. Kinetic lactate dehydrogenase assay for detection of cell damage in primary neuronal cell cultures. *Bio-Protocol* 2017; 7: e2308.
- Endres M, Gertz K, Lindauer U, et al. Mechanisms of stroke protection by physical activity. *Ann Neurol* 2003; 54: 582–590.
- Koch S, Mueller S, Foddiss M, et al. Atlas registration for edema-corrected MRI lesion volume in mouse stroke models. *J Cereb Blood Flow Metab* 2019; 39: 313–323.
- Donath S, AJ, Lee SL, et al. Interaction of ARC and daxx: a novel endogenous target to preserve motor function and cell loss after focal brain ischemia in mice. *J Neurosci* 2016; 36: 8132–8148.
- Emmrich JV, Neher JJ, Boehm-Sturm P, et al. Stage 1 registered report: Effect of deficient phagocytosis on neuronal survival and neurological outcome after temporary

- Middle cerebral artery occlusion (tMCAo). *Fl000Res* 2017; 6: 1827.
32. Maurice T, Hiramatsu M, Kameyama T, et al. Behavioral evidence for a modulating role of sigma ligands in memory processes. II. Reversion of carbon monoxide-induced amnesia. *Brain Res* 1994; 647: 57–64.
  33. Schlunk F, Fischer P, Princen HMG, et al. No effects of PCSK9-inhibitor treatment on spatial learning, locomotor activity, and novel object recognition in mice. *Behav Brain Res* 2021; 396: 112875.
  34. Zhao W, Zhang X and Rong J. SUMOylation as a therapeutic target for myocardial infarction. *Front Cardiovasc Med* 2021; 8: 701583.
  35. Knauss S, Albrecht C, Dirnagl U, et al. A semiquantitative non-invasive measurement of PcomA patency in C57BL/6 mice explains variance in ischemic brain damage in filament MCAo. *Front Neurosci* 2020; 14: 576741.
  36. Rosonina E, Akhter A, Dou Y, et al. VS, Regulation of transcription factors by sumoylation. *Transcription* 2017; 8: 220–231.
  37. Yao JS, Zhai W, Young WL, et al. Interleukin-6 triggers human cerebral endothelial cells proliferation and migration: the role for KDR and MMP-9. *Biochem Biophys Res Commun* 2006; 342: 1396–1404.
  38. Mitchell AS, Czajkowski R, Zhang N, et al. Retrosplenial cortex and its role in spatial cognition. *Brain Neurosci Adv* 2018; 2: 2398212818757098.
  39. Marshel JH, Garrett ME, Nauhaus I, et al. Functional specialization of seven mouse visual cortical areas. *Neuron* 2011; 72: 1040–1054.
  40. Wirtshafter HS and Wilson MA. Lateral septum as a nexus for mood, motivation, and movement. *Neurosci Biobehav Rev* 2021; 126: 544–559.
  41. Sharpe MJ and Killcross S. The prelimbic cortex directs attention toward predictive cues during fear learning. *Learn Mem* 2015; 22: 289–293.
  42. Kuffner MTC, Koch SP, Kirchner M, et al. Paracrine interleukin 6 induces cerebral remodeling at early stages After unilateral common carotid artery occlusion in mice. *Front Cardiovasc Med* 2021; 8: 805095.